molecules

MDPI

Review

Research Progress of Non-Noble Metal Catalysts for Carbon Dioxide Methanation

Yingchao Cui [1,†], Shunyu He [1,†], Jun Yang [2], Ruxing Gao [1,*], Kehao Hu [2], Xixi Chen [2], Lujing Xu [2], Chao Deng [2], Congji Lin [1], Shuai Peng [1] and Chundong Zhang [2,*]

[1] School of Energy Science and Engineering, Nanjing Tech University, Nanjing 211816, China; cuiyingchao@njtech.edu.cn (Y.C.); 202361108022@njtech.edu.cn (S.H.); lincj@njtech.edu.cn (C.L.); 202121008109@njtech.edu.cn (S.P.)

[2] State Key Laboratory of Materials-Oriented Chemical Engineering, College of Chemical Engineering, Nanjing Tech University, Nanjing 211816, China; 202121104510@njtech.edu.cn (J.Y.); 202161104182@njtech.edu.cn (K.H.); c.xx@njtech.edu.cn (X.C.); xulujing@njtech.edu.cn (L.X.); dengc@njtech.edu.cn (C.D.)

* Correspondence: grxing@njtech.edu.cn (R.G.); zhangcd@njtech.edu.cn (C.Z.)

† These authors contributed equally to this work.

Abstract: The extensive utilization of fossil fuels has led to a rapid increase in atmospheric CO_2 concentration, resulting in various environmental issues. To reduce reliance on fossil fuels and mitigate CO_2 emissions, it is important to explore alternative methods of utilizing CO_2 and H_2 as raw materials to obtain high-value-added chemicals or fuels. One such method is CO_2 methanation, which converts CO_2 and H_2 into methane (CH_4), a valuable fuel and raw material for other chemicals. However, CO_2 methanation faces challenges in terms of kinetics and thermodynamics. The reaction rate, CO_2 conversion, and CH_4 yield need to be improved to make the process more efficient. To overcome these challenges, the development of suitable catalysts is essential. Non-noble metal catalysts have gained significant attention due to their high catalytic activity and relatively low cost. In this paper, the thermodynamics and kinetics of the CO_2 methanation reaction are discussed. The focus is primarily on reviewing Ni-based, Co-based, and other commonly used catalysts such as Fe-based. The effects of catalyst supports, preparation methods, and promoters on the catalytic performance of the methanation reaction are highlighted. Additionally, the paper summarizes the impact of reaction conditions such as temperature, pressure, space velocity, and H_2/CO_2 ratio on the catalyst performance. The mechanism of CO_2 methanation is also summarized to provide a comprehensive understanding of the process. The objective of this paper is to deepen the understanding of non-noble metal catalysts in CO_2 methanation reactions and provide insights for improving catalyst performance. By addressing the limitations of CO_2 methanation and exploring the factors influencing catalyst effectiveness, researchers can develop more efficient and cost-effective catalysts for this reaction.

Keywords: CO_2 hydrogenation; methanation; thermocatalysis; non-noble metal catalysts; mechanism

check for updates

Citation: Cui, Y.; He, S.; Yang, J.; Gao, R.; Hu, K.; Chen, X.; Xu, L.; Deng, C.; Lin, C.; Peng, S.; et al. Research Progress of Non-Noble Metal Catalysts for Carbon Dioxide Methanation. *Molecules* **2024**, *29*, 374. https://doi.org/10.3390/molecules29020374

Academic Editor: Stefano Falcinelli

Received: 25 December 2023
Revised: 7 January 2024
Accepted: 8 January 2024
Published: 11 January 2024

Copyright: © 2024 by the authors. Licensee MDPI, Basel, Switzerland. This article is an open access article distributed under the terms and conditions of the Creative Commons Attribution (CC BY) license (https://creativecommons.org/licenses/by/4.0/).

1. Introduction

Fossil fuels have been extensively used since the Industrial Revolution, which has not only promoted social progress but also brought about global energy shortages and environmental pollution [1]. The massive emission of greenhouse gases, particularly CO_2, has continuously raised the global average temperature, resulting in the rise of sea levels, the melting of glaciers, and the frequent occurrence of extreme climate events in recent years [2]. Controlling carbon emissions is an important strategic measure for the international community and governments to deal with these problems [3,4]. However, fossil fuels still account for the main body of the energy structure, and it is difficult to achieve effective control of CO_2 in the short term [5]. At the same time, CO_2 is an important C1 resource, which can be captured and reacted with hydrogen to realize resource utilization [6],

which can not only reduce carbon emissions but also obtain high-value-added chemical products [7,8], and carbon capture and storage (CCS) is also largely mature at the technical level [9].

CO_2 conversion pathways include photocatalysis, electrocatalysis, and thermal catalysis [10]. Thermal catalysis requires a relatively low reaction temperature, produces few by-products, and has a high conversion rate [11]. In recent years, with the development and utilization of renewable energy, hydrogen can be obtained from electrolytic water, wind energy, solar energy, etc. [12]. Hydrogen is stable and renewable; its energy is high; and it can react with CO_2 to achieve a low-carbon cycle [13]. The reaction of CO_2 with hydrogen can produce formic acid, methane, methanol, dimethyl ether, and its derivatives [14,15]. The methanation process of CO_2 is simple, and the reaction conditions are mild [16]. Methane can be used as fuel or a raw material for other chemicals [17,18]. Moreover, the methane generated can be directly transported by the existing natural gas pipeline network [19]. Therefore, it has high research value in realizing the large-scale application of CO_2 hydrogenation in industry.

CO_2 methanation is an exothermic reaction, and it is more favorable to the reaction at low temperatures, but the dynamics limit its industrial application [20]. It was originally used to remove trace amounts of CO and CO_2 from H_2-rich feed gas to prevent catalytic poisoning [21]. With the emergence of the oil crisis, CO_2 methanation was expected to generate methane as a substitute for natural gas, but due to the low reaction rate, low CO_2 conversion, and low CH_4 selectivity, CO_2 methanation has not been used on a large scale in the industry [22]. In recent years, CO_2 methanation has been extensively studied, and various scholars have explored the mechanism, kinetics, and thermodynamics of the reaction and studied the design of the reactor to improve the reaction efficiency [23]. Finding suitable catalysts to increase the rate of the CO_2 methanation reaction and improve CO_2 conversion and CH_4 selectivity is the focus of research [24].

At present, the most studied catalysts for CO_2 methanation are noble metal catalysts and non-noble metal catalysts. Noble metal catalysts mainly include Ru, Rh, Pt, Pd, Au, etc. [25]. Although noble metal catalysts show high activity, they are generally expensive, which is not suitable for large-scale use in industry [26]. Non-noble metal catalysts are mainly Ni, Co, Fe, Mo, etc. [27]. The Ni-based catalyst has been widely studied for its high methanation activity, strong hydrogen adsorption capacity, and low price [28]. However, it is prone to sintering at higher temperatures and oxidation atmospheres, so the modification of catalysts is needed to improve its catalytic performance [29]. For example, it has been found that reducing the size of Ni particles and increasing their dispersion can improve their activity [30]. In addition, the Co-based catalyst has high catalytic activity, stability, and coking resistance, but it needs appropriate reaction conditions to achieve good conversion [31]. The Fe-based catalyst has good reaction activity and a low price, but the reaction requires being carried out under high temperatures and pressures, CH_4 selectivity needs to be improved, and it is easy to accumulate carbon [32,33]. The Mo-based catalyst has perfect vulcanization resistance and can also be used for CO_2 methanation [34], but its activity is low in the reaction. Therefore, different catalysts have different limitations. To improve their performance in CO_2 methanation reactions, it is generally possible to adjust the loading of active metal [35], select appropriate supports [36,37], choose the best preparation method [38], and add promoters [39–41]. In addition, reaction conditions such as temperature, pressure, space velocity, and the H_2/CO_2 ratio also affect their reaction activity [42], so appropriate reaction conditions should be selected in the research.

In this work, we review the performance of non-noble metal catalysts commonly used in CO_2 methanation reactions based on the above content. First, the kinetic and thermodynamic properties of CO_2 methanation are discussed. It is shown that the reaction is thermodynamically favorable at low temperatures and high pressure. From the kinetic perspective, it is found that too-low temperatures will reduce the reaction rate, so it is necessary to find catalysts that can maintain activity at low temperatures. After that, we discuss the effect of reaction conditions on catalyst activity. The appropriate reaction

conditions (temperature, pressure, space velocity, and H_2/CO_2 ratio) are beneficial to the reaction. Then we explain and discuss the effect of support material, preparation methods, and promoters on the catalyst performance for Ni-based, Co-based, Fe-based, and Mo-based catalysts, respectively. Moreover, we also provide some ideas for the modification of the catalyst to improve the catalytic performance. Finally, we review the reaction mechanisms of CO_2 methanation, namely the CO intermediate mechanism and the formate intermediate mechanism.

2. CO_2 Methanation Thermodynamics and Kinetics

Thermodynamic analysis of chemical reactions is used to analyze whether the reaction can proceed, the chemical equilibrium state of the reaction, the thermodynamic equilibrium limit, etc. The thermodynamic reaction equation for the CO_2 methanation reaction is shown in Equation (1) [43].

$$CO_2 + 2H_2 \rightarrow CH_4 + 2H_2O,\ \Delta rH_m^{\Theta} = -165.0\ kJ{\cdot}mol^{-1} \quad (1)$$

$$\Delta G = \Delta H - T\Delta S,\ \Delta_r G_m^{\Theta} = -113.6\ kJ{\cdot}mol^{-1} \quad (2)$$

where $\Delta_r H^{\Theta}{}_m$ is the standard heat of reaction and $\Delta_r G^{\Theta}{}_m$ is the standard Gibbs free energy difference; Equation (2) is the Gibbs free energy equation, and the Gibbs free energy difference is negative, indicating that the reaction can be carried out spontaneously, which suggests that the CO_2 methanation reaction is feasible on a thermodynamic level.

In addition to the main reaction of Equation (1), the CO_2 methanation process contains the following side reactions:

$$CO + 3H_2 \rightarrow CH_4 + H_2O,\ \Delta H_{298K} = -206\ kJ \cdot mol^{-1} \quad (3)$$

$$CO_2 + H_2 \rightarrow CO + H_2O,\ \Delta H_{298K} = +41\ kJ \cdot mol^{-1} \quad (4)$$

$$CO_2 + CH_4 \rightarrow 2CO + 2H_2,\ \Delta H_{298K} = +247\ kJ{\cdot}mol^{-1} \quad (5)$$

$$2CO \rightarrow C + CO_2,\ \Delta H_{298K} = -172\ kJ \cdot mol^{-1} \quad (6)$$

$$CH_4 \rightarrow C + 2H_2,\ \Delta H_{290K} = +75\ kJ \cdot mol^{-1} \quad (7)$$

$$CO + H_2 \rightarrow C + H_2O,\ \Delta H_{298K} = -131\ kJ \cdot mol^{-1} \quad (8)$$

$$CO_2 + 2H_2 \rightarrow C + 2H_2O,\ \Delta H_{298K} = -90\ kJ \cdot mol^{-1} \quad (9)$$

Obviously, it is necessary to inhibit the occurrence of side reactions in order to ensure the high selectivity of CH_4 (Equations (3)–(9)). A number of thermodynamic analyses of the CO_2 methanation reaction have been carried out using the Gibbs minimization principle. It is shown that when the temperature is lower than 600 °C, the CO_2 conversion rate decreases with the increase in temperature and increases with the increase in pressure. At 1 standard atmospheric pressure, when the temperature is greater than 600 °C, the CO_2 conversion rate gradually increases with the increase in temperature, which may be attributed to the occurrence of the reverse water gas shift (RWGS) reaction, leading to the conversion of CO_2. When the reaction temperature is 200~500 °C, the CH_4 selectivity remains stable. However, the CH_4 selectivity decreases with the increase in temperature when the temperature exceeds 500 °C [44]. Thus, an appropriate temperature and pressure is beneficial for the reaction to proceed. Massa et al. [45] found that the introduction of water vapor into the

system slightly reduces CH_4 yield, but it inhibits the carbon build-up to a certain extent. Baamran et al. [43] investigated the effect of different parameters such as temperature, pressure, and phenol concentration on the generation of H_2, CO_2, CO, CH_4, and H_2O. The results showed that high-temperature conditions are more favorable for the generation of H_2 and CO, while CH_4 is more likely to be generated at low temperatures. Finally, a series of coking reactions occur at high temperatures, which mainly lead to catalyst deactivation.

Through thermodynamic aspects, it appears that CO_2 methanation is thermodynamically favorable at low temperatures and high pressures. However, there are multiple fundamental steps that are often catalyst dependent, and kinetic limitations are often the hurdles that must be overcome first, which requires a thorough understanding of the fundamental mechanistic steps of CO_2 methanation to identify the key kinetic steps that can be addressed through process operation or catalyst design.

It was found that the rate of methanation of CO_2 depends more on the H_2 partial pressure than on the CO_2 partial pressure at low CO_2 conversion levels. Chanpon et al. [46] have established the dependence of the rate of CO_2 methanation on the partial pressures of the reactants and products at different temperatures with 1.5 mg of Ni/Al_2O_3 catalyst diluted in SiC, and the results show that the CH_4 formation is highly dependent on the H_2 concentration at the CO_2 partial pressure of 22 kPa (Figure 1), while the dependence on the CO_2 partial pressure is weak.

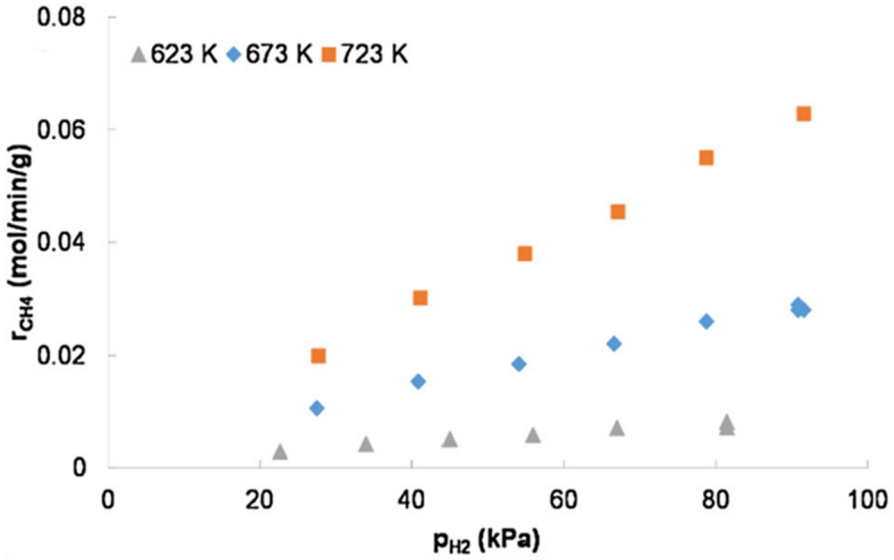


Figure 1. Effect of partial pressure on CO_2 methanation on 1.5 mg Ni/Al_2O_3 5 mg Ni/Al_2O_3 catalyst in SiC, 115 kPa total pressure and $1.06 \cdot 10^6 \cdot h^{-1}$ at 623 K-130 kPa total pressure and $3.16 \cdot 10^6 \cdot h^{-1}$ at 673 K and 723 K with H_2 at 22 kPa CO_2 partial pressure [46]. Copyright (2019) Journal of CO_2 Utilization.

Based on the thermodynamic analysis, it was found that suitable low temperatures, pressurization, and a high H_2/CO_2 molar ratio are conducive to increasing the yield of the target product (CH_4). The reaction kinetics analysis showed that too low a temperature would reduce the reaction rate, so the catalyst was required to maintain the activity at a low temperature to reduce energy consumption during the reaction and shorten the reaction time. In addition, the current industrial methanation process usually adopts an adiabatic fixed-bed reactor, and every 1% of CO_2 conversion would bring about an adiabatic temperature rise of about 60 °C to the system, and even with a larger product gas circulation, it was still difficult to avoid the existence of local hot spots in the catalyst. Even with a large product gas recycling volume, localized hot spots in the bed are still unavoidable. Therefore, methanation catalysts with low-temperature activity and high-

temperature stability need to be developed to meet the demands of industrial production. The basic steps of CO_2 methanation are shown in Table 1.

Table 1. Basic steps of CO_2 methanation proposed via the CO formation pathway (left) and the formate formation pathway (right) (s refers to surface sites) [42]. Copyright (2021) Catalysis Today.

CO Formation Path Way	Formate Formation Path Way
$H_2, g + 2s = 2H_{-s}$ (1a)	$H_2, g + 2s = 2H_{-s}$ (2a)
$CO_2, g + 2s = CO_{-s} + O_{-s}$ (1b)	$CO_2, g + s = CO_{2-s}$ (2b)
$CO_{-s} = CO, g + s$ (1c)	$CO_{2-s} + H_{-s} = HCOO_{-s} + s$ (2c)
$CO_{-s} + s = C_{-s} + O_{-s}$ (1d)	$HCOO_{-s} + H_{-s} = HCO_{-s} + OH_{-s}$ (2d)
$C_{-s} + 4H_{-s} = CH_{4-s} + 4s$ (1e)	$HCO_{-s} + H_{-s} = CH_{-s} + OH_{-s}$ (2e)
$CH_{4-s} = CH_4, g + 4s$ (1f)	$CH_{-s} + 3H_{-s} = CH_4, g + 4s$ (2f)
$O_{-s} + 2H_{-s} = H_2O + 2s$ (1g)	$OH_{-s} + H_{-s} = H_2O, g + 2s$ (2g)

3. Optimization of Reaction Conditions

The CO_2 methanation reaction is highly sensitive to reaction conditions. Optimizing reaction conditions can significantly improve reaction conversion, selectivity, and product distribution. A complete understanding of these crucial factors can further benefit kinetic evaluation, process optimization, reactor design, and scale-up for industrial applications [47]. In this section, the role of operating conditions such as temperature, pressure, gas hourly space velocity (GHSV), and the H_2/CO_2 ratio is extensively discussed.

3.1. Effect of Reaction Temperature

The standard enthalpy and the standard Gibbs free energy of the Sabatier reaction (Equation (10)) are $\Delta H^{\theta}_{298K} = -165\ kJ \cdot mol^{-1}$ and $\Delta G^{\theta}_{298K} = -142\ kJ \cdot mol^{-1}$, respectively [47]. Thermodynamically, this is favored at low temperatures (25~400 °C) [48], and the reaction is exothermic. However, the reduction of carbon in the fully oxidized state of CO_2 to CH_4 is an eight-electron process with obvious kinetic constraints [49], which requires catalysts and appropriate temperatures to improve the rate and selectivity of the reaction.

Fan et al. [50] investigated the effect of temperature on the distribution of CO_2 methanation products by using a micron/nano TiO_2 catalyst. They found that CH_4 and H_2O were the main products at lower temperatures (150~400 °C), while the production of CO gradually increased when the temperature exceeded 450 °C. The reason for this change may be that the RWGS reaction (Equation (1)) favors and dominates at high temperatures. González-Castaño et al. [51] synthesized a series of Ni/γ-Al_2O_3, Ni-Fe/γ-Al_2O_3, and Ni-Fe-K/γ-Al_2O_3 catalysts and evaluated them by methanation experiments. They concluded that the CO_2 conversion of each catalyst exhibited a volcanic-shaped tendency with an increase in temperature. The reaction rate reached equilibrium conversion at about 450 °C (Figure 2). However, when the temperature was higher than 450 °C, the CO_2 conversion decreased, obviously due to catalyst deactivation (sinter, agglomeration) and coking [52].

In addition, the low-temperature conversion of CO_2 methanation on non-noble metal catalysts has been one of the research hotspots in recent years. For example, Zhu et al. [53] prepared a Y_2O_3-promoted NiO-CeO_2 catalyst by designing the oxygen vacancy of the Ni-based catalyst. They introduced the metal oxide Y_2O_3, which is incompatible with the support CeO_2 lattice, to promote the generation of oxygen defects. Under mild conditions (<300 °C), the catalyst was three times more active than the conventional NiO/CeO_2 catalyst. Ma et al. [54] found that the turnover frequency (TOF) of CO_2 methanation of Ni/monoclinic-ZrO_2 was increased by 116% compared with that of Ni/cubic-ZrO_2 at 240 °C by optimizing the crystal phase of ZrO_2 in the Ni/ZrO_2 catalyst, while the activation energy of the reaction was reduced by 24%.

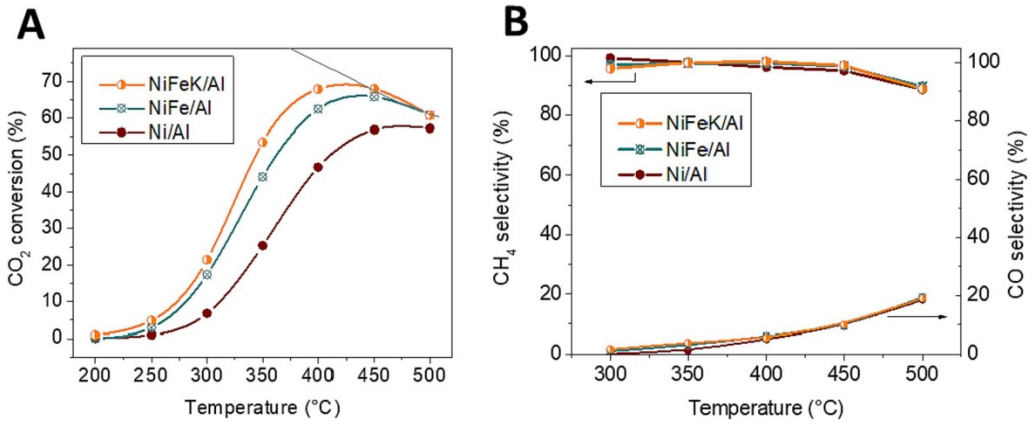


Figure 2. For CO_2 methanation, catalytic activity at 9 L CO_2 $g^{-1}{\cdot}h^{-1}$ and H_2: CO_2 = 4: (**A**) CO_2 conversion; (**B**) %CH_4 selectivity and %CO selectivity [51]. Copyright (2023) Fuel.

3.2. Effect of Reaction Pressure

The CO_2 methanation reaction is a gaseous reaction in which the number of reactants is reduced. According to Le Chatelier's law, pressurization is an effective measure to improve the conversion rate. Thermodynamic studies conducted by Ahmad et al. [55] on the Cu-K/Al_2O_3 catalyst showed that the equilibrium conversion and CH_4 yield increased with the increase in pressure and were more sensitive under high pressure. Yarbaş et al. [56] conducted modeling and studied the equilibrium composition of the reaction pressure at 1, 3, 5, and 10 atm, respectively (Figure 3). It was found that the proportion of CH_4 in the products at all pressures reached its maximum at the lowest temperature (100 °C), and the trend of species changes with temperature was consistent at all pressures. With the increase in pressure, the molar concentration of the reactants (CO_2 and H_2) decreased, while the molar concentration of the products (CH_4 and H_2O) increased at the same temperature.

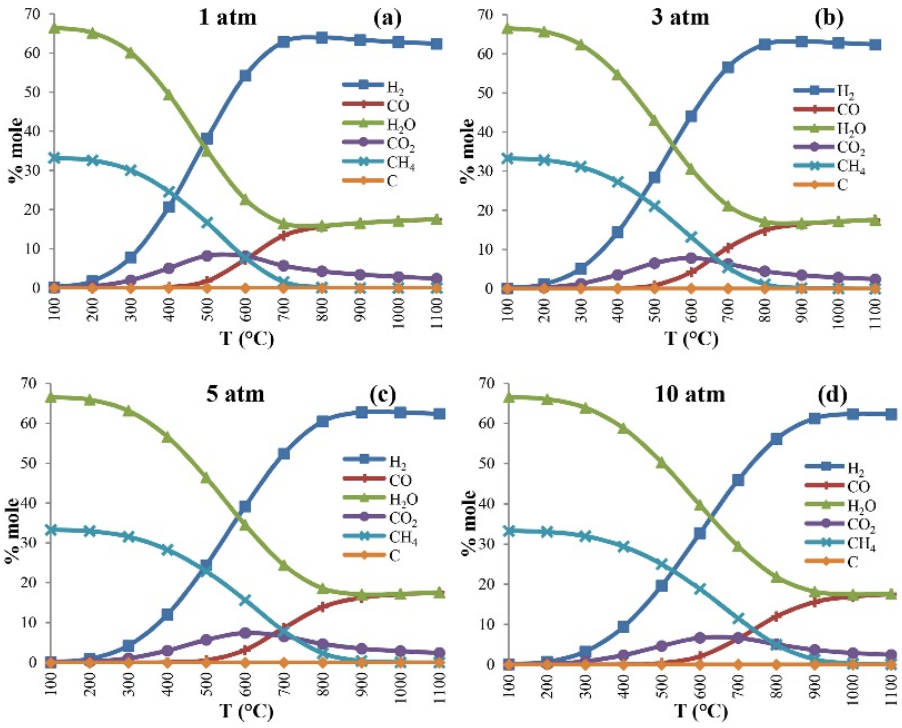


Figure 3. The equilibrium compositions of different cases; (**a**) P = 1, (**b**) P = 3, (**c**) P = 5, and (**d**) P = 10 atm [56]. Copyright (2023) International Journal of Hydrogen Energy.

Theoretically, higher CO_2 conversion and CH_4 selectivity can be achieved under conditions of low temperature and high pressure. However, from an industrial perspective, high-pressure equipment is more dangerous to use, and the low-temperature reaction rate is lower. Therefore, the optimal conditions for CO_2 methanation are a temperature of 30~500 °C and a pressure of 0.1~0.3 MPa [57].

3.3. Effect of Gas Hourly Space Velocity

GHSV is also an important factor affecting the performance of catalysts. For instance, Mihet's team reported that lower GHSV could improve the catalytic performance of CO_2 methanation. This is because the lower GHSV directly translates into a longer residence time [58], which increases the contact and reaction time of the catalyst with the reactant feedstock gas. In addition, appropriate GHSV can take away the heat generated in the methanation reaction, and it is not easy to cause excessive temperature and deactivate the catalyst [59].

However, too high GHSV will shorten the residence time of CO_2 on the catalyst surface, which will reduce the conversion rate. For example, Fan et al. [50] discussed the catalytic performance of methanation on a 15% Ni/TiO_2 catalyst when the GHSV increased from 6200 to 18,600 $mL \cdot g^{-1} \cdot h^{-1}$ (Figure 4). It was found that the catalytic performance decreased significantly when the GHSV was 18600 $mL \cdot g^{-1} \cdot h^{-1}$, which is because not all CO_2 can be successfully adsorbed and converted into CH_4 at the active sites of the catalyst at high reaction flow rates. Due to the limited active sites available for the hydrogenation reaction, limiting the conversion of CO_2 and production of CH_4.

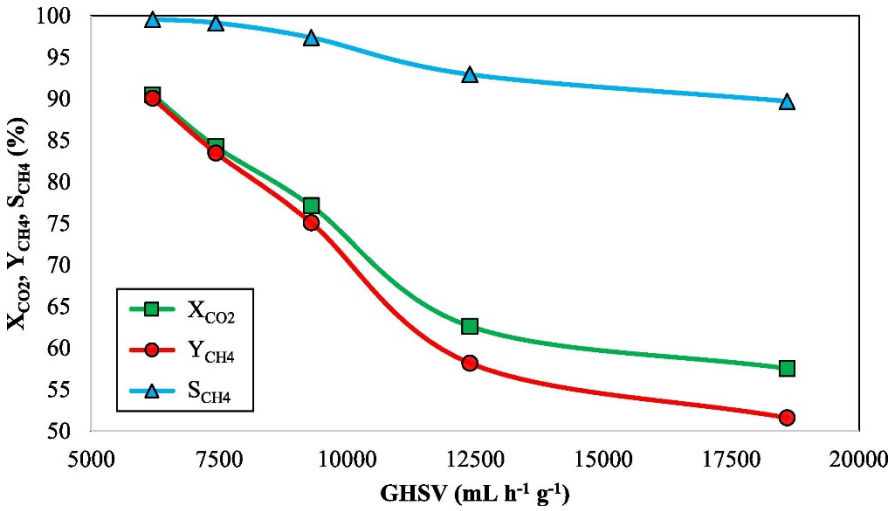


Figure 4. Catalytic performance of 15% Ni/TiO_2 at 350 °C and atmospheric pressure under different GHSV [50]. Copyright (2022) Energy Conversion and Management.

3.4. Effect of H_2/CO_2 Ratio

According to the study [55], the H_2/CO_2 ratio has an important influence on the CO_2 methanation reaction in terms of CO_2 conversion, CH_4 yield, and CO and CH_4 selectivity. For example, Jaffar et al. [60] prepared a 10% Ni/Al_2O_3 catalyst and explored the effect of the H_2/CO_2 ratio on the CO_2 methanation reaction in detail by changing the molar ratio of H_2/CO_2. The results showed that when the H_2/CO_2 ratio increased from 2 to 4, the CO_2 conversion and CH_4 selectivity increased from 29.1% and 88.9% to 71.7% and 96.1%, respectively, and the methane concentration increased from 5.8 mmol to 9.3 mmol (Figure 5). However, when the H_2/CO_2 ratio reached 4.5, the CO_2 conversion and CH_4 yield dropped. This is consistent with the conclusions reached by Aziz et al. [61] and Moghaddam et al. [62]. The possible reason is that when the H_2/CO_2 ratio is greater than 4, the excess H_2 molecules on the catalyst surface compete for CO_2 adsorption, reducing the active sites available for CO_2 adsorption.

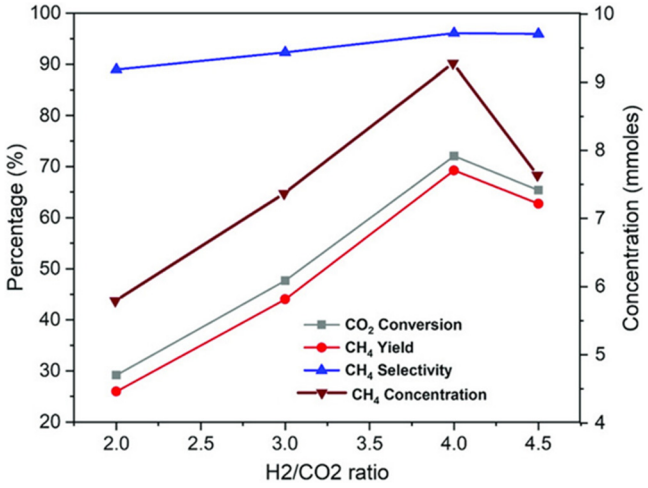


Figure 5. Effect of H_2: CO_2 ratio on CH_4 concentration, CO_2 conversion, CH_4 selectivity, and CH_4 yield [60]. Copyright (2019) Energy Technology.

In addition, the H_2/CO_2 ratio also affects the carbon deposition of the catalyst. According to the thermodynamic experiments conducted by Gao et al. [44] on the Ni-based catalyst, when the H_2/CO_2 ratio is as low as 2, up to 50% carbon deposition can be observed at 500 °C, while when the H_2/CO_2 ratio is equal to or greater than 4, the carbon deposition decreases to 0. Hussain et al. [57] conducted evaluation experiments and thermodynamic studies on the CO_2 methanation reaction of a metal-free fibrous silica-β zeolite (FS@SiO_2-BEA) catalyst. It was found that when the H_2/CO_2 ratio increased from 1 to 2, the proportion of CH_4 in the product increased and the proportion of CO decreased. On further increasing the ratio from 2 to 3, the molar fraction of coke formation decreased remarkably, and when the ratio increased to 4, the molar fraction of coke became 0. Based on this observation, it can be concluded that a high H_2/CO_2 ratio is conducive to high CH_4 and no carbon generation.

4. Non-Noble Metal Catalysts for CO_2 Methanation Reaction

4.1. Ni-Based Catalysts

The catalysts used for CO_2 methanation are mainly supported by Group VIII metals, with active metals, including Ru, Rh, Pd, Pt, Fe, Co, Ni, etc. [63]. Among them, Ni-based catalysts have been widely studied in the process of CO_2 methanation due to their high catalytic activity, high CH_4 selectivity, abundant reserves, and low price [64].

Ni-based single-atom catalysts have extremely high activity in the activation of C–H bonds, but the carbon deposition generated by C–H bond activation will cover the Ni active sites, resulting in catalyst deactivation [65]. Therefore, it is necessary to further enhance the catalytic activity and CH_4 selectivity of Ni-based catalysts, such as through the application of supports and promoters, the use of appropriate preparation methods, etc. [66].

4.1.1. Support

The support material affects the activity of the catalyst by improving the dispersion of the active component, adjusting the surface structure of the catalyst, and affecting the strong interaction between the support and the active component [67]. For Ni-based catalysts, conventional oxide supports include Al_2O_3, SiO_2, TiO_2, CeO_2, and ZrO_2, and other supports include zeolites, MOFs, etc. [68].

Al_2O_3 has been extensively used for CO_2 methanation due to its high specific surface area and relatively low cost [69]. Chen et al. [70] prepared the NiMn/Al_2O_3 catalyst with various Mn loadings and found that the addition of Mn could improve the dispersion of Ni and facilitate the formation of CH_4. Moreover, 20Ni2Mn/Al_2O_3 has more basic sites, which was conducive to the adsorption and activation of CO_2, and the CO_2 conversion

(90.5%) was the highest at 250 °C. In this study, Al_2O_3 was detected in the calcined catalyst, and Ni species were all present as NiO compounds. The Mn phase is highly dispersed, and no corresponding diffraction peaks were observed using XRD. For the reduced catalysts, Mn species were mainly present in the form of MnO_2, and Ni became difficult to detect, a phenomenon that suggests that the Mn additives led to a better dispersion of Ni particles in the samples.

SiO_2 generally exists in an amorphous state and has easily regulated average pore diameter, specific surface area, and pore volume [71]. Xu et al. [72] prepared the Ni-HMS catalysts using hexagonal mesoporous silica (HMS) as the support by the one-pot method. Compared with Ni/HMS and Ni/SiO_2 catalysts prepared by traditional methods, the 15Ni-HMS catalyst has the highest CO_2 conversion and CH_4 selectivity (99.9%) (see Figure 6). The Ni-HMS mesoporous framework can anchor Ni active sites to inhibit sintering, and Ni particles are highly dispersed, which effectively improves the performance of the catalyst. Wang et al. [38] prepared the catalytic activity of Ni/SiO_2 catalysts with different Ni particle sizes by different preparation methods and investigated the effect of Ni particle sizes on CO_2 methanation in the range of 3.5~7.5 nm. As shown in Figure 7, the Ni particles of all samples were spherically supported on SiO_2 supports, but the catalysts prepared by different methods showed different particle sizes. The catalytic performance of Ni/SiO_2 catalysts with different Ni particle sizes is shown in Figure 8. It can be seen that the ED catalyst with the smallest nickel particle (3.5 nm) has the highest CO_2 conversion rate and the best CH_4 yield in the temperature range of 200~500 °C. The characterization results showed that reducing the size of Ni particles can increase the adsorption of CO_2 and the number of active sites, thus improving the catalytic activity.

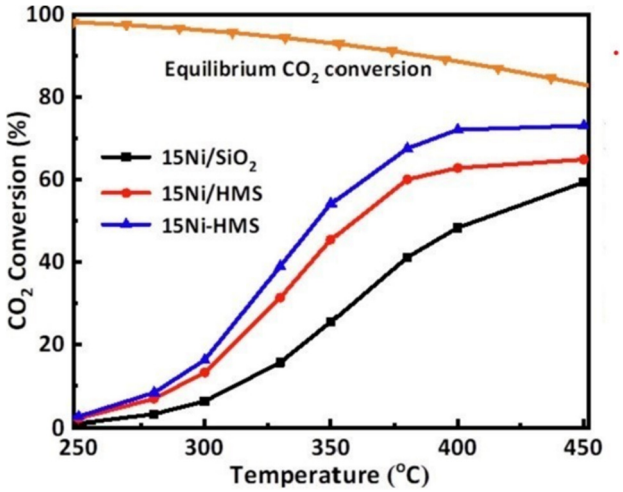


Figure 6. The curves of the CO_2 conversion versus the reaction temperature over the 15Ni-HMS, 15Ni/HMS, and 15Ni/SiO_2 catalysts [72]. Copyright (2023) Fuel.

TiO_2 can promote the dissociation of the C–O bond and CO_2 hydrogenation activity by electronic interaction with metals [73]. Unwiset et al. [74] prepared Ni/TiO_2 catalysts with different loads of Ni by the sol–gel method and found that the 20 wt% Ni/TiO_2 catalyst had the best activity and stability, in which CH_4 selectivity was almost 100% and CO_2 conversion was reduced by less than 10% at 420 °C for 72 h. This can be attributed to the fact that increasing Ni helped Ni^{2+} replace Ti^{4+} in the lattice. Moreover, TiO_2 deformation generates more oxygen vacancies, inhibits the growth of TiO_2 crystals, reduces the crystal size, and thus increases the specific surface area of the catalyst. Li et al. [75] found that due to the strong metal–support interaction (SMSI) that induced a TiO_2 coating around Ni nanoparticles, the catalytic activity of CO_2 methanation of the Ni-based catalyst on the traditional anatase support was inhibited. However, a large amount of Ti^{3+} will be produced after pretreatment of a-TiO_2 with NH_3 and H_2, which can hinder the formation of

titanium coating and change SMSI, so that the reactants can be exposed to more Ni species and enhance the catalytic activity of Ni/a-TiO_2.

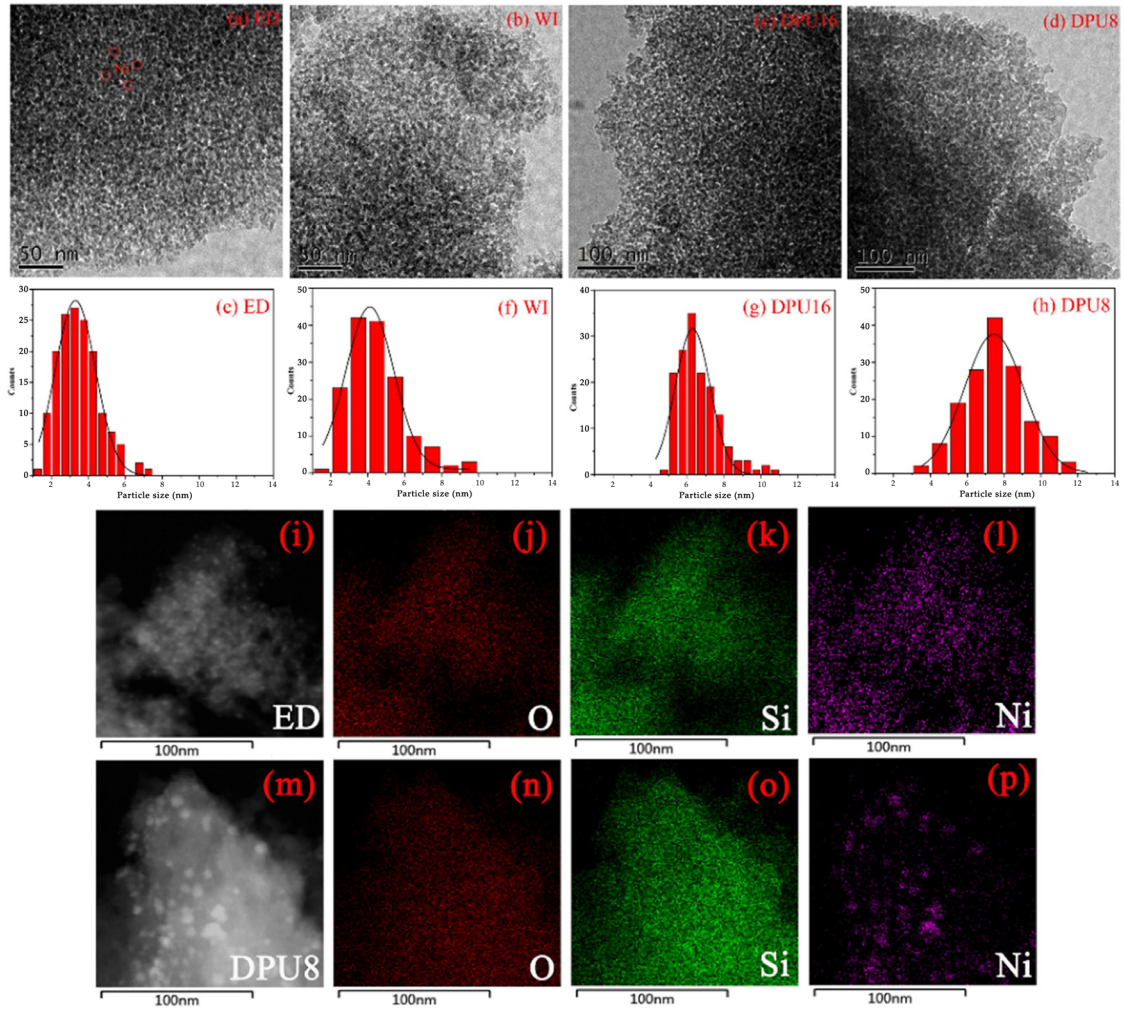


Figure 7. TEM images (**a**–**d**,**i**,**m**) of reduced Ni/SiO_2 catalysts and the statistics particle size distribution (**e**–**h**). EDS mapping of ED (**j**–**l**) and DPU8 (**n**–**p**) [38]. Copyright (2021) Fuel.

ZrO_2 has abundant active and basic sites on its surface, good thermal stability, and high porosity [64]. Espino et al. [76] studied the performance of Ni/ZrO_2, Ni/Mg(Al)O, and Ni/SiO_2 catalysts in the CO_2 methanation reaction and found that the Ni/ZrO_2 catalyst has the highest CO_2 conversion rate and CH_4 selectivity (98%), as shown in Figure 9. Due to the insertion of Ni into the ZrO_2 lattice and its own defects, oxygen vacancy was generated, which improved the adsorption and dissociation of CO on the Ni/ZrO_2 catalyst.

CeO_2 has a high specific surface area and abundant oxygen vacancy [77]. Bian et al. [78] prepared Ni-based catalysts with different CeO_2 morphologies by the hydrothermal method, namely 5Ni/NPs, 5Ni/NOs, 5Ni/NCs, and 5Ni/NRs. They found that these supports have type IV isotherms, as shown in Figure 10, indicating a rich mesoporous structure from nanocrystal aggregation. They also found that the 5Ni/NPs catalyst had abundant oxygen vacancy, appropriate metal–support interaction, and the best catalytic activity and stability. Moreover, the CO_2 conversion rate order below 300 °C was 5Ni/NPs > 5Ni/NOs > 5Ni/NCs > 5Ni/NRs, indicating that the morphology of the CeO_2 support affected the activity of the catalyst. Li et al. [79] compared the catalytic activity of Fe/CeO_2, Co/CeO_2, and Ni/CeO_2 for CO_2 hydrogenation and found that Ni/CeO_2 had the highest CO_2 conversion rate, and the selectivity of Ni/CeO_2 and Co/CeO_2 for CH_4 was almost 100%. In contrast, Fe/CeO_2 tended to produce CO. The strong interaction between Fe and

CeO_2 can promote the activation of CO_2 but weaken the activation of H_2, resulting in poor CO_2 hydrogenation activity, while the moderate interaction between Ni, Co, and CeO_2 is conducive to H_2 activation, thus enhancing the catalytic activity.

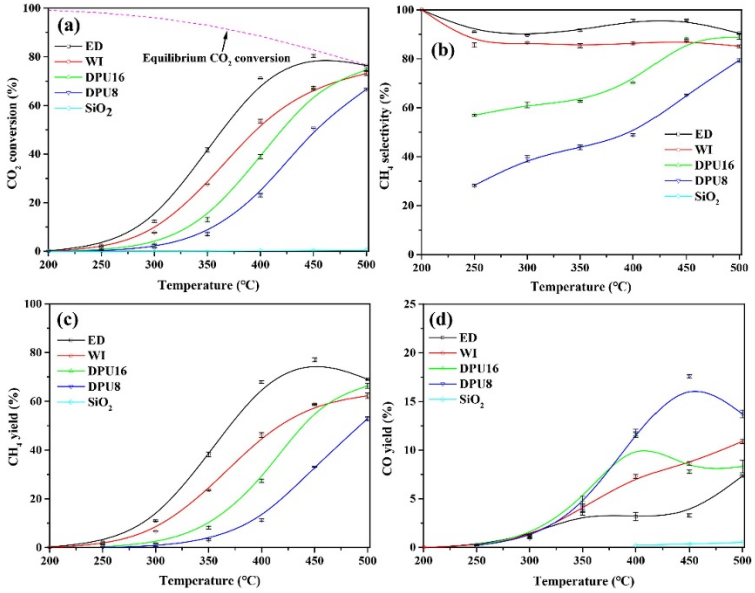


Figure 8. Activity data expressed as CO_2 conversion and equilibrium CO_2 conversion (**a**), CH_4 selectivity (**b**), CH_4 yield (**c**), CO yield (**d**). Experimental conditions: catalyst mass = 0.1 g, T = 200–500 °C, feed flow = 20 mL/min (2 mL/min CO_2, 8 mL/min H_2, 10 mL/min N_2), GHSV = 12,000 h^{-1} [38]. Copyright (2021) Fuel.

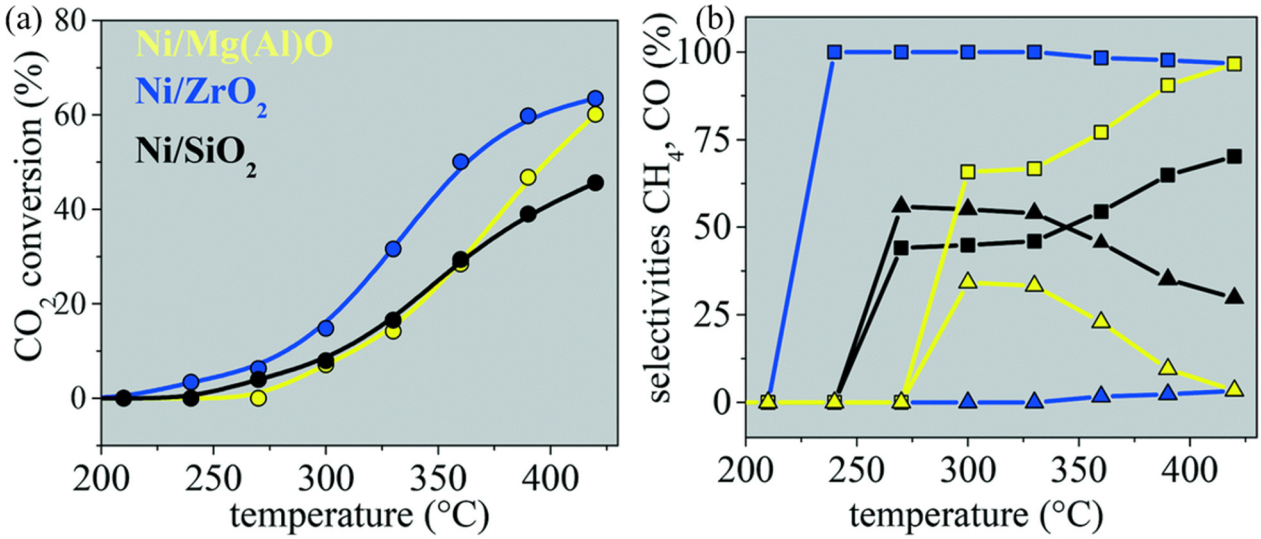


Figure 9. (**a**) CO_2 conversion versus temperature. The blue, yellow, and black symbols represent Ni/ZrO_2, Ni/Mg(Al)O, and Ni/SiO_2, respectively. The experimental conditions are as follows: catalyst mass 200 mg, H_2/CO_2 ratio 4:1, flow rate 80 mL·min^{-1}, and pressure 1 atm. (**b**) Selectivity to CH_4 (squares) and CO (triangles) versus temperature. The catalyst colors and the experimental conditions are the same as in (**a**) [76]. Copyright (2022) Catalysis Science & Technology.

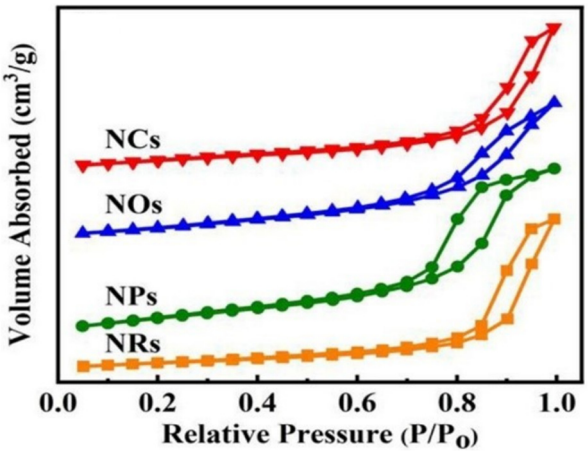


Figure 10. N_2 adsorption–desorption isotherms of the as-prepared NRs, NCs, NPs, NPs supports [78]. Copyright (2023) Fuel.

Metal–organic frameworks (MOFs) are a kind of crystalline porous material with a periodic network structure composed of metal ions or metal clusters and organic ligands. It has the advantages of porous structure, large specific surface area, regular pore morphology, flexible composition and structure, etc., so it has been widely used in CO_2 catalytic reduction [80]. Compared with traditional catalysts, MOFs can give catalysts unique morphology, flexible and predictable structure, and uniform element distribution [81]. Lin et al. used a high-surface-area Al-containing metal–organic framework, MIL-53 (Al), as a sacrificial support to obtain Ni-Al_2O_3 catalysts with 5 to 20 wt% Ni content. It was found that Ni nanoparticles were highly dispersed in MOF-derived catalysts, and the formation after MOF calcination of nickel aluminate nanodomains was beneficial to improving the activity and stability of the catalyst [82]. Feng et al. pointed out that the smaller the size of Ni particles, the more active sites can be exposed, which is more favorable for improving catalytic activity. However, small particles are prone to aggregation during impregnation, and particle agglomeration can be inhibited by inhibiting the growth of metal nanoparticles through the carrier pores, while MOFs can be used to limit the supported nanoparticles to maintain small sizes in the pores. They synthesized a MOF-derived Ni/CeO_2 catalyst and obtained highly dispersed ultra-fine Ni nanoparticles by using the constraint effect of the porous structure of MOFs. Calcination at 600 °C increased the number of oxygen vacancies in the Ni/CeO_2 catalyst, thereby improving the adsorption capacity of CO_2 and the catalytic performance [83].

4.1.2. Preparation Method

Different preparation methods may affect the grain size of the active component and the metal–support interaction, leading to different catalytic performances. The common catalyst preparation methods include impregnation, co-precipitation, sol–gel, hydrothermal, and deposition-precipitation.

The co-precipitation method can be used to prepare non-noble metal oxide catalysts with high metal content, but the performance of the catalyst will be affected by solution concentration, pH, feeding sequence, and stirring intensity. Zhang et al. [84] prepared Ni/CeO_2 catalysts by a continuous co-precipitation method and found that catalysts prepared by the improved co-precipitation method have better low-temperature CO_2 methanation activity than catalysts prepared by the impregnation method, as shown in Figure 11.

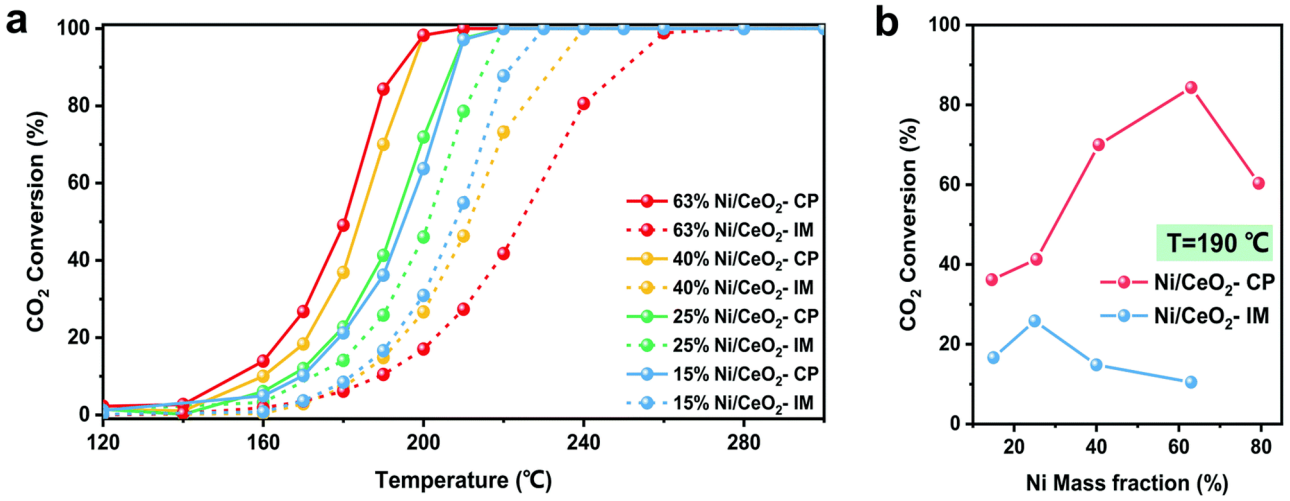


Figure 11. (**a**) CO_2 methanation activities of the catalysts prepared by the CP/IM method with different Ni loadings at various temperatures (reaction conditions: P = 1.0 atm, SV = 24,300 $mL \cdot g^{-1} \cdot h^{-1}$, ($H_2/CO_2$) molar ratio = 80), (**b**) comparison of CO_2 conversion for catalysts with different Ni loadings at 190 °C [84]. Copyright (2022) Catalysis Science & Technology.

The active metal of catalysts prepared by the sol–gel method is relatively well-dispersed. Moghaddam et al. [85] used a new sol–gel method without surfactants to synthesize an Ni/Al_2O_3 catalyst with 15~30 wt% Ni content. It was found that the specific surface area of the catalyst was large, up to 269.2 to 297.3 $m^2 \cdot g^{-1}$, and the Ni is easier to reduce due to the weak interaction between NiO and Al_2O_3. Moreover, $30Ni/Al_2O_3$ had the best catalytic performance at 350 °C, the CO_2 conversion was 73.98%, and the CH_4 selectivity was 99%. The catalyst samples after 700 °C calcination were mainly cubic nickel aluminate spinel, and no NiO peaks were detected even at higher Ni content, suggesting that Ni is highly dispersed.

The catalyst prepared by the hydrothermal method has good dispersion, uniform distribution, and light particle agglomeration and is commonly used to synthesize catalysts with controllable morphology. Liu et al. [86] compared the performance of Ni/SiO_2 catalysts prepared by impregnation, the sol–gel method, and hydrothermal methods. It was found that the Ni particle size on the catalyst prepared by the hydrothermal method was the smallest and the dispersion was the best, and there were more active sites on the surface of the catalyst, resulting in better catalytic performance.

In addition to those mentioned above, there are several preparation methods. For example, the active components of the catalyst obtained by impregnation can be evenly distributed in the pores of the support. However, it may cause the migration of active components during the drying process [87]. The deposition–precipitation method can improve the utilization rate of active components but requires a high specific surface area of the support, and the metal particles generated are larger and the uniformity is low [88].

4.1.3. Promoter

Adding various kinds of metal promoters to Ni-based catalysts can improve the dispersion of active components on the surface of the catalyst to regulate the relationship between the active components and support, thereby improving the activity and stability of catalysts. The promoters of Ni-based catalysts mainly include alkaline earth metals, transition metals, and rare earth metals [89].

Liu et al. [90] modified Ni/CeO_2 by doping alkaline earth metals (Mg, Ba, Sr, and Ca) and found that the activity of Ni/CeO_2 was improved. The activity order of catalysts was $Ni/Ca_{0.1}Ce_{0.9}O_x$ > $Ni/Sr_{0.1}Ce_{0.9}O_x$ > $Ni/Mg_{0.1}Ce_{0.9}O_x$ > $Ni/Ba_{0.1}Ce_{0.9}O_x$ > Ni/CeO_2, and the CO_2 conversion of $Ni/Ca_{0.1}Ce_{0.9}O_x$ was 75% at 290 °C, CH_4 selectivity was 99%. The chemical characterization of catalysts showed that adding alkaline earth metal oxides

was beneficial to improve the dispersion of Ni, and there were more oxygen vacancies on the surface of $Ni/M_{0.1}Ce_{0.9}O_x$, which was related to medium basic sites on the surface of catalysts.

The transition metals Ti, Mn, Fe, Co, and Cu have unique acid–base and reduction properties. Akash et al. [91] compared the CO_2 methanation reaction on 17 wt% Ni/γ-Al_2O_3 and 17 wt% $Ni_{3.2}Fe/\gamma$-Al_2O_3 catalysts and found that adding Fe could improve the stability of Ni^0, and Fe inhibited the formation of CO^* or the adsorption of CO. The 17 wt% $Ni_{3.2}Fe/\gamma$-Al_2O_3 catalyst had a higher CO_2 conversion of 42%. Shafiee et al. [92] modified Ni-Al_2O_3 by adding different contents of Co and found that the activity of catalysts was improved. As shown in Figure 12, increasing the content of Co could increase the CO_2 conversion. The 15Ni-12.5Co-Al_2O_3 has the best catalytic performance, with CO_2 conversion at 76.2% at 400 °C and CH_4 selectivity at 96.39%.

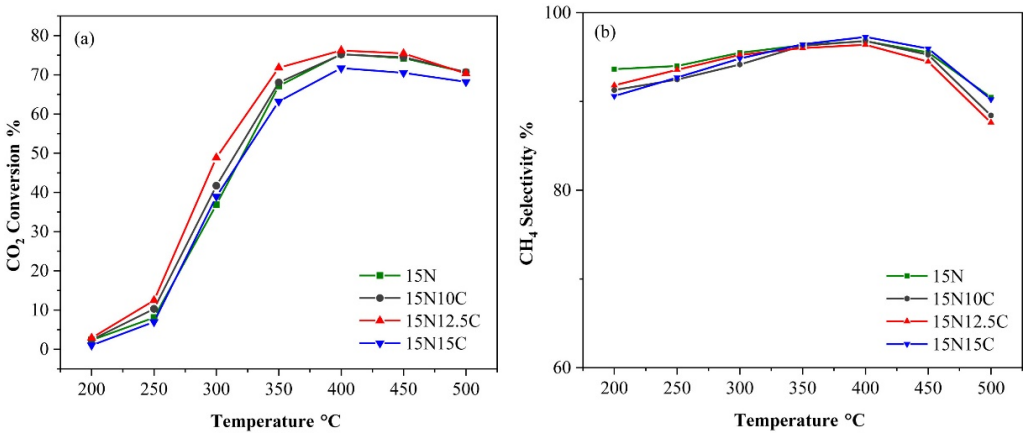


Figure 12. Effect of cobalt loadings on (**a**) CO_2 conversion and (**b**) CH_4 selectivity of the 15Ni-Co-Al_2O_3 catalysts calcined at 500° with (GHSV = 9000 $mL \cdot g_{cat}^{-1} \cdot h^{-1}$, ($H_2/CO_2$) molar ratio = 4) [92]. Copyright (2021) International Journal of Hydrogen Energy.

Reihaneh Daroughegi et al. [93] studied the effect of adding Zr, Ce, La, and Mo on the performance of Ni-Al_2O_3 catalysts and found that the catalysts with added promoters had higher Ni content and better reducibility at high temperatures and could also improve the interaction between Ni and Al_2O_3. Among them, the 25Ni-5Ce-Al_2O_3 catalyst had the smallest Ni crystal size, and Ni could be highly dispersed. The addition of Zr and Ce could promote the formation of oxygen vacancies on the catalyst, thereby enhancing the adsorption capacity of CO_2.

4.2. Co-Based Catalysts

Co and Ni belong to the group VIII elements; the activity of hydrogenation reactions is strong for both of them. However, Co catalysts have a poor ability to catalyze the water–gas shift (WGS) reaction. On the other hand, in the CO_2 hydrogenation reaction, Co can not only be used as a promoter for Ni-based catalysts but also as an active component itself [94,95]. Because of the weak activity of Co in the WGS reaction, the amount of CO_2 adsorbed on the surface of Co is very low, resulting in a small C/H ratio on the surface and the easy formation of CH_4, which has the characteristics of less carbon deposition and high selectivity. Considering the characteristics of cost, applicability, stability, and activity, the Co catalyst has certain research significance.

4.2.1. Supports

The support has a crucial influence on the activity of Co-based catalysts. Through the strong interaction between the carrier and Co particles, the redox properties and adsorption properties of the catalyst are affected, and the performance of the catalyst is changed [49].

At present, Co-based catalysts mostly use metal oxides such as ZrO_2, Al_2O_3, SiO_2, TiO_2, zeolite molecular sieves, and other polymer porous materials.

Among them, the most studied Co/Al_2O_3 and Co/ZrO_2 catalysts have the closest and highest CH_4 yields. The Co/ZrO_2 catalyst has higher activity, CO_2 conversion, and stability when it is close to equilibrium. Li et al. loaded 10 wt% Co on ZrO_2 by the impregnation method, and the activity remained after 300 h and the selectivity of CH_4 reached 99.9% [96]. Al_2O_3 has a wide range of sources and is easy to prepare. The $FeCo/Al_2O_3$ catalyst exhibits excellent catalytic performance under mild reaction conditions (280 °C, 0.2 MPa), whose reaction rate was 8.7 μmol $g_{cat}{}^{-1}{\cdot}s^{-1}$, under the synergistic effect of Al_2O_3 support and Fe, the yield is significantly higher than that of Co/Al_2O_3 catalyst ($1.68{\cdot}10^{-3}$ $mol{\cdot}g_{cat}{}^{-1}{\cdot}min^{-1}$) [97]. In this study, researchers used in situ XRD to follow the intermediate-state products of Co and Fe. As for samples with equal amounts of FeCo, there was an apparent metallic Fe^0 phase at 600 °C, and Fe_3O_4 and $CoFe_3O_4$ were detected. Although there was no CoO/Co phase detected, the presence of metallic Fe^0 definitely indicated the existence of interaction and the improvement of reducibility.

Lauterbach et al. [98,99] compared the interaction of SiO_2, Al_2O_3, and TiO_2 supports with cobalt nanorods (CoNR) materials. In the kinetically controlled temperature range (150~250 °C), the $CoNR/TiO_2$ catalyst exhibited higher catalytic activity than the other two catalysts. Whereas, in the temperature range of mass transfer control (>300 °C), $CoNR/Al_2O_3$ exhibits significantly enhanced activity due to the good thermal conductivity of Al_2O_3. Compared with $CoNR/TiO_2$ and $CoNR/Al_2O_3$, $CoNR/SiO_2$ shows no change in catalytic activity compared with pure CoNR, indicating that the promotion effect of SiO_2 support was not obvious.

In the direction of zeolite material support, Nadia et al. [100] prepared a special methanation catalyst by using Co-based layered zeolitic imidazolate framework (ZIF-L) material under an argon atmosphere, that is, fixed on highly porous nitrogen Co nanoparticles in a doped carbon matrix. The specific activity of the catalyst at 350 °C is 22.3 $mol_{CH4}{\cdot}g_{cat}{}^{-1}{\cdot}min^{-1}$, which is significantly better than more conventional ZIF-67-like catalysts (11.7 $mol_{CH4}{\cdot}g_{cat}{}^{-1}{\cdot}min^{-1}$). This is due to the stability of Co nanoparticles (~20 nm) and the abundant basic active sites associated with nitrogen doping in ZIF-L-prepared catalysts. What is more, this new catalyst has not been observed to be deactivated within 60 h, which shows the high stability of the catalyst.

4.2.2. Preparation Method

In order to obtain a highly dispersed catalyst, the preparation method is also an important part of the activity of the catalyst. On the idea of preparing Co/ZrO_2 catalyst by the impregnation method, Li et al. [95] adopted the method of organic acid-assisted preparation to obtain a highly dispersed Co/ZrO_2 catalyst. The loading of Co in the carrier was only 2 wt%, but the CO_2 methanation reaction exhibits excellent catalytic performance. Among many organic acids, the Co/ZrO_2 catalyst prepared by citric acid has the best catalytic activity, and the conversion of CO_2 is as high as 85%, see in Figure 13. At the same time, citric acid-assisted preparation of Co/diatomite catalysts is also an effective method to improve the performance of the catalyst. The CO_2 conversion is 73%, the CH_4 selectivity is 96%, and it shows good stability in the long-term reaction [101]. The assistance of organic acids can effectively improve the metal dispersion of Co catalysts and thus obtain more active sites for CO_2 adsorption and catalytic hydrogenation.

Anastasiia et al. [102] synthesized a mesoporous m-Co_3O_4 catalyst with a BET surface area of 95 $m^2{\cdot}g^{-1}$ using the co-precipitation method. And found that the m-Co_3O_4 catalyst was more active than the commercial c-Co_3O_4 (BET surface area of 15 $m^2{\cdot}g^{-1}$) catalyst and had better thermal stability at high temperatures, see in Figure 14. This study shows that in the CO_2 methanation reaction, factors such as the morphology of the catalyst body and surface and the existence of defect sites directly affect the catalytic performance and reaction mechanism of the catalyst [48].

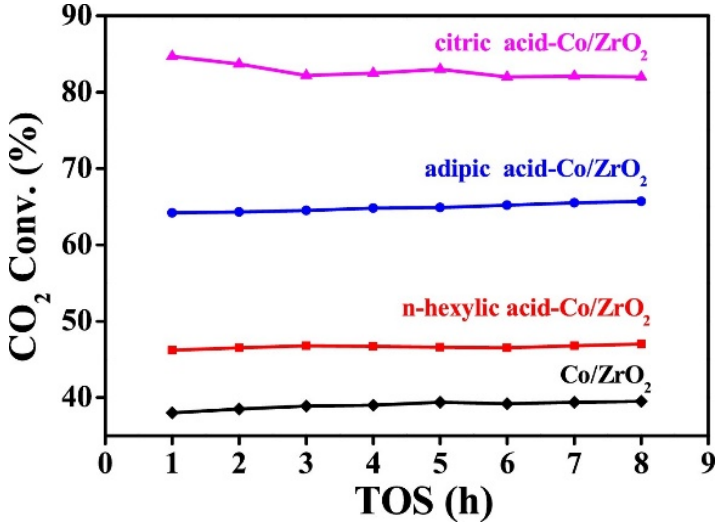


Figure 13. The catalytic performance of n-hexylic acid, adipic acid, and citric acid-assisted Co/ZrO_2 catalysts and the benchmark Co/ZrO_2 catalyst. Conditions: molar ratio of $H_2/CO_2 = 4/1$, GHSV = 7200 $mL \cdot g^{-1} \cdot h^{-1}$, P = 3 MPa, T = 400 °C [95]. Copyright (2019) Applied Catalysis B-Environmental.

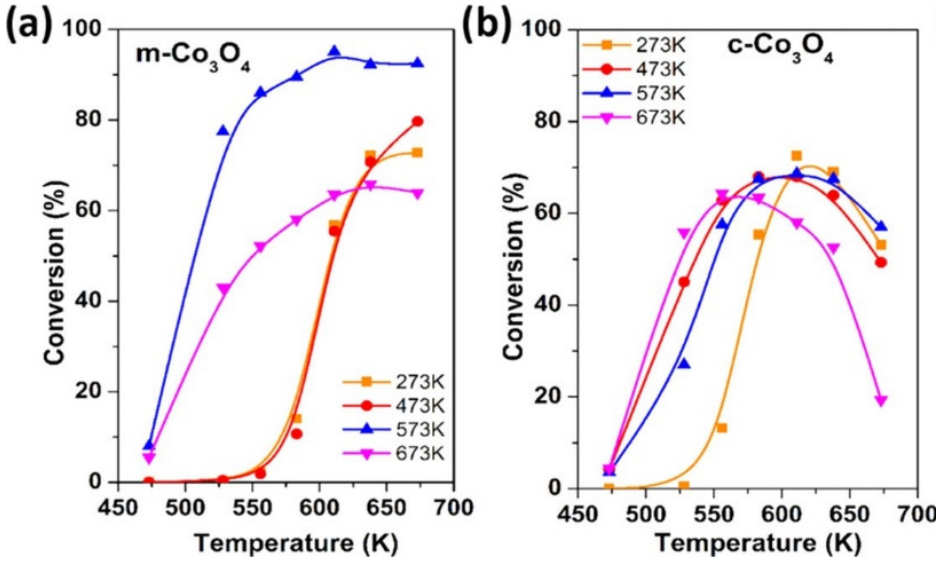


Figure 14. CO_2 conversion over (**a**) m-Co_3O_4 and (**b**) c-Co_3O_4 reduced at 273, 473, 573, and 673 K [102]. Copyright (2021) Journal of Physical Chemistry C.

Compared with the impregnation method, the catalysts prepared by the co-precipitation method have a stronger interaction between Co oxide and Ce. For the preparation of Co/CeO_2 catalysts, a moderate calcination temperature is a reasonable condition to achieve high CASA (catalytically active surface area), but when the calcination temperature of co-precipitated and impregnated catalysts is 500~700 °C, the total number of basic sites will significantly decrease [103]. DFSP (double flame spray pyrolysis) enables the control and separation of the particle formation process of different catalyst components and can be used to evaluate the effects of active metals, support materials, dopants, and promoters, as well as particle size distribution and porosity. Max Gäßler et al. [104] used DFSP technology to support Co nanoparticles with the same particle size distribution on SiO_2, TiO_2, and SiO_2-TiO_2 mixtures, and obtained the activity, selectivity, and deactivation behavior of the supported Co catalysts from the support materials main conclusions.

4.2.3. Promoter

Jakob Stahl et al. [105] used the DFSP method to synthesize catalysts with different promoters with the same size distribution and dispersion to study the co-catalytic effect of Pt, ZrO_x, SmO_x, and other promoters on Co-based catalysts. Among them, ZrO_2 and Pt performed significantly better than SmO_x, as shown in Figure 15. With the introduction of the Pt promoter, the H_2 absorption rate and the corresponding metal surface area are significantly increased, while the CO_2 adsorption capacity is similar to that of the Co catalyst without the promoter.

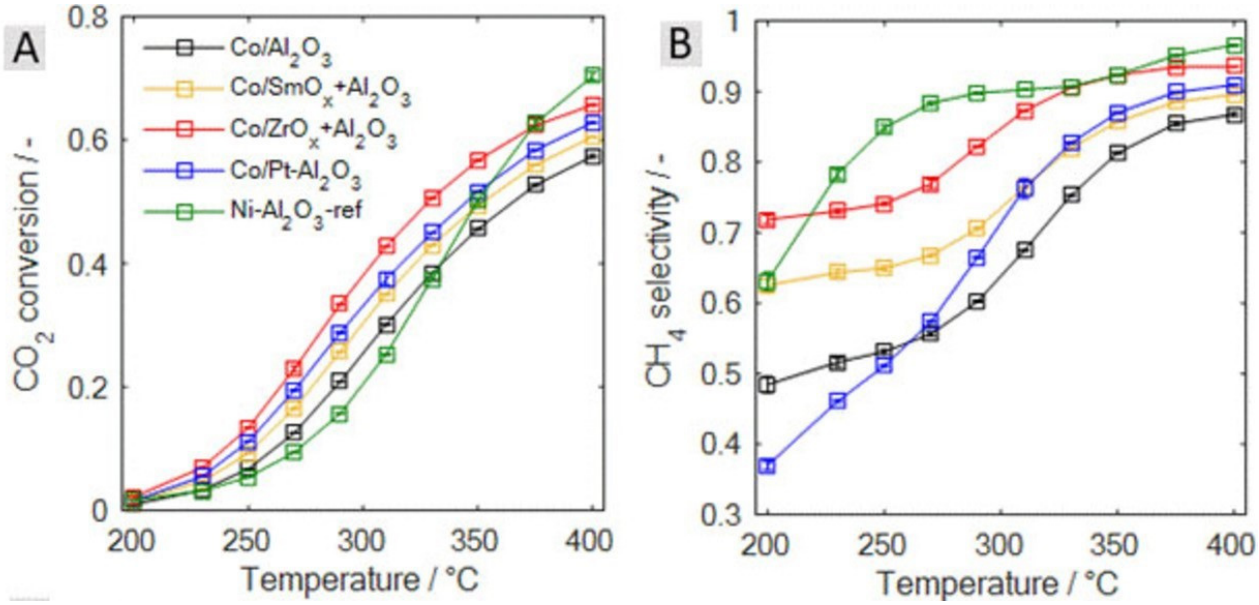


Figure 15. Results of the CO_2 methanation experiments for all studied catalysts. (**A**) CO_2 conversion vs. temperature; (**B**) CH_4 selectivity vs. temperature. Conditions: total pressure 1 bar, total flow rate 50 mLS·min^{-1} composed of 4/1/5 H_2/CO_2/Ar, 25 mg of catalyst [105]. Copyright (2021) ChemCatChem.

In order to achieve high-efficiency catalysis of CO_2 methanation by non-noble metal catalysts at low temperatures (<200 °C), Tu et al. [106] found that by adding Zr to amorphous Co catalysts, the low-temperature catalytic effect was similar to that of noble metals. Since the Zr promoter can expand the surface area of the catalyst, adjust the valence state of the surface atoms of the catalyst, and combine with the rich surface defects and inherent active sites brought about by the amorphous nature of the catalyst itself, high-efficiency catalysis at low temperatures is realized.

The addition of an Mn promoter can significantly improve the performance of Co-based catalysts, which not only promotes the overflow of hydrogen from active Co sites to spinel supports but also leads to a significant increase in the catalytic active surface area of Mn-modified catalysts [107].

4.3. Other Catalysts

In addition to Ni-based and Co-based catalysts, supported Fe-based catalysts are also commonly used as active catalysts for CO_2 hydrogenation. Because traditional Ni-based catalysts are inactivated by sintering under high-temperature conditions, Fe-based catalysts are non-toxic, cheaper, and easier to obtain. They have a higher specific surface area and can react at lower pressures [97].

Similar to the above, the catalytic performance of Fe-based catalysts depends to a large extent on synthesis methods, such as impregnation, coprecipitation, sol–gel, etc. [108]. For instance, Güttel et al. [109] prepared α-Fe_2O_3 catalysts, Fe-based catalysts supported by

SiO_2 (15Fe/SiO_2), and core–shell catalysts (15Fe@SiO_2), and compared their CO_2 methanation activity. The α-Fe_2O_3 and 15Fe/SiO_2 catalysts were all prepared by the impregnation method, while the core–shell 15Fe@SiO_2 catalyst was obtained by the adaptive inverse microemulsion method [110]. The experimental results show that under the reaction condition of 400 °C, 1 bar, with a space velocity of 52,000 h^{-1}(69.2 mmol(CO_2)/mol(Fe)/s) and H_2/CO_2 = 4, the CH_4 generation rate of the α-Fe_2O_3 and 15Fe/SiO_2 catalysts is similar, which is 0.25 $mmol_{(CO2)}\cdot(mol_{(Fe)}\cdot s)^{-1}$ and the 15Fe@SiO_2 catalyst has better stability. Combined with the characterization technology, it was found that there is no carbon deposition on the 15Fe@SiO_2 catalyst with a core–shell structure after reaction for 17 h without the reaction process of hot sintering, and the core–shell structure is complete [109]. However, the depletion of α-Fe_2O_3 samples is subjected to breakage or wear, and the stability is not high [111]. They pointed out that the methanation activity of the 15Fe@SiO_2 catalyst needs to be improved, but its carbon deposition is about 300 times less than that of the α-Fe_2O_3 catalyst and 32 times lower than that of impregnated Fe-based catalysts, their TEM plots are shown in Figure 16. Moreover, the stability of 15Fe@SiO_2 catalysts is significantly improved [109].

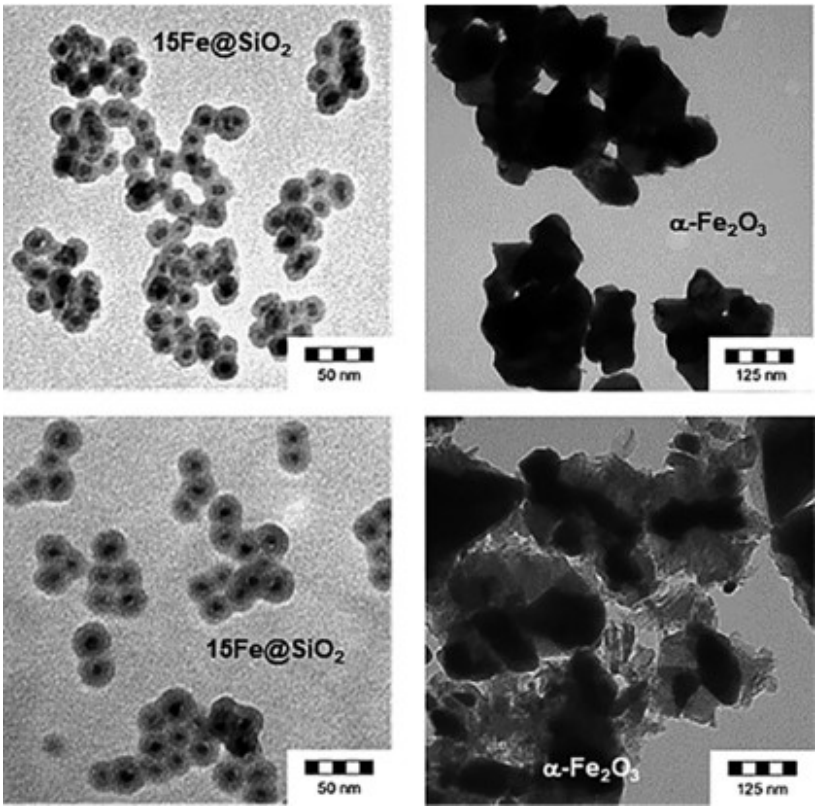


Figure 16. Preparation (**top**) and consumption (**bottom**) of TEM micrographs of α-Fe_2O_3 and 15Fe@SiO_2 sample preparation [109]. Copyright (2020) Chemie Ingenieur Technik.

In addition, TiO_2, SiO_2, ZrO_2, and Al_2O_3 are commonly used as metal oxide supports for catalysts in methanation reactions. Toemen et al. [112] synthesized a novel metal oxide (Ru/Fe/Ce) on the γ-Al_2O_3 catalyst by the impregnation method and investigated the methanation activity under atmospheric pressure. They compared the various properties of Ru/Fe/Ce γ-Al_2O_3 catalysts at different calcination temperatures. It was found that the Ru/Fe/Ce (5:10:85)/γ-Al_2O_3 catalysts calcined at 900 °C had a higher specific surface area (73.87 $m^2\cdot g^{-1}$) than those calcined at 1000 °C (51.07 $m^2\cdot g^{-1}$) and 1100 °C (22.30 $m^2\cdot g^{-1}$). The increase in calcination temperature will reduce the specific surface area and pore volume of the catalyst. When the temperature rises to 1100 °C, the larger the pore size and the smaller the pore volume, the lower the catalytic activity. Therefore, the 10 g

Ru/Fe/Ce (5:10:85)/γ-Al_2O_3 catalyst calcined at 1000 °C has a higher catalytic activity, the CO_2 conversion rate is increased to 100%, and the CH_4 yield is 90.5%. In addition to the above oxides, zeolite can also be used as the carrier of Fe-based catalysts, and the interaction between the two can improve the dispersion of Fe species. For instance, using zeolite as the support of Fe-based catalysts, Franken et al. [113] studied the impregnation method to prepare three catalysts with different loading loads (1, 5, and 10 wt%) and analyzed the zeolite structure with relevant characterization. It was found that the impregnation process and calcination temperature had a great impact on the stability of zeolite. The results show that the reaction rate is 42 $mmol_{(CO2)}\cdot(mol_{(Fe)}\cdot s)^{-1}$ and the selectivity of CH_4 is 76% with a loading of 1 wt% at 300 °C and 10 bar. When the loading of Fe is high, it tends to form more and more high-carbon hydrocarbons in Fischer–Tropsch reaction products under increased pressure. In addition, the catalysts with high Fe loading are more likely to destroy the zeolite structure and form Fe_3C around the support, which affects the selectivity of CH_4. Therefore, avoiding the formation of the Fe_3C phase is crucial for the high selectivity of CH_4.

Promoters are also an important part of the catalyst and have an important impact on the activity of the catalyst. For example, Kureti et al. [114] prepared a series of Fe-based catalysts with different Mg contents, deeply explored the influence of promoters on the methanation reaction of Fe-based catalysts, and found that Mg as a promoter could further enhance catalyst activity by improving the basicity of the catalyst surface and greatly improving the CO_2 conversion rate. The results showed that when the load of Mg is 2 wt%, the highest CH_4 yield is 32% and the selectivity is 65%. In addition, Landau et al. [115] studied the effects of TiO_2, SiO_2, ZrO_2, and MnO on the hydrogenation of CO_2 in the presence of the surfactant cetyl trimethyl ammonium bromide (CTAB). The results showed that TiO_2 at 20 wt% increased the rate of RWGS and FTS. The selectivity of CO was decreased and that of CH_4 was increased, which is conducive to the methanation reaction.

In addition to the Fe-based catalyst mentioned above, the Mo-based catalyst has good sulfide performance and can be used for methanation reactions [116]. Qin et al. [117] found that Mo/Al_2O_3 catalysts are widely used in chemical production, but the interaction between Mo and Al_2O_3 is not strong enough under high-temperature methanation reactions, and the dispersion of MoS_2 supported by Al_2O_3 is poor, which makes it easy to sinter in the reaction. The interaction between Mo and CeO_2 is stronger than that between Mo and Al_2O_3. The Mo phase supported on CeO_2 tends to exist in the form of monolayer MoS_2, but highly dispersed MoS_2 is unstable. CeO_2/Al_2O_3-supported MoS_2 catalysts have high dispersion and excellent high-temperature stability. The effects of the roasting method and precipitation method on the preparation of CeO_2 on the Mo-based catalyst are compared by relevant characterization methods, and the results show that the catalytic activity and stability of the CeO_2 support prepared by the roasting method are higher [118]. Wang et al. [119] prepared MoO_3/CeO_2 catalysts by the impregnation method. They studied the effect of MoO_3 loading on methanation catalytic performance and found that the CO conversion rate reached its maximumwhen 5 wt% MoO_3 was added to CeO_2 support. Wang et al. [120] reported that MoP catalysts were widely used in CO hydrogenation reactions, and a series of MOP-x (x = P/Mo ratio from 1 to 5) catalysts were prepared by pyrolysis of phytic acid (PA)-derived Mo complexes in H_2 atmosphere. The physicochemical properties and catalytic activity of MoP catalysts were studied, and the characterization results further confirmed that the $Mo^{\delta+}$ site of MoP catalysts is the active site of methanation reactions, and its content on the surface of MOP-x catalysts determines the catalytic activity of the catalysts. In addition, Cu-based catalysts are also used as catalysts for CO_2 hydromethanation. Gabor Varga et al. [121] prepared an efficient Cu–Co bimetallic catalyst for CO_2 methanation through a spinel oxide precursor system and found that $Cu_{0.4}Co_{2.6}O_4$ showed high activity and high CH_4 selectivity (65–85%) in the temperature range of 250~425 °C. However, Cu-based catalysts are mostly used for CO_2 hydrogenation electrocatalytic conversion or CO_2 hydrogenation to methanol.

5. Reaction Mechanisms

An in-depth understanding of key intermediates and reaction mechanisms is critical for the design of catalysts [122]. Many researchers have elucidated possible CO_2 methanation mechanisms through in situ FTIR, mass spectrometry (MS) techniques, and density functional theory (DFT) calculations. Although there is much debate about the intermediates and different reaction pathways for the generation of CH_4, these mainly include the following two pathways: (1) The CO pathway, also known as CO_2 dissociation methanation: chemisorbed $*CO_2$ can dissociate into *CO and *O. The formed *CO can be further dissociated into carbon (*C) and then hydrogenated to CH_4 by desorption of the dissociated H_2 on the metal particles from the catalyst surface, while *O can react with hydrogen to form H_2O. (2) Formic acid pathway: The formic acid substance is the main intermediate product formed in the CO_2 methanation reaction, also known as CO_2-associated methanation: Chemisorbed $*CO_2$ is first converted to didentate (HCOO*), then to formic acid (HCOOH), and then to CH_4 [48,123–128]. The possible reaction pathways are shown in Figure 17. In addition to the above two pathways, there are other pathways, such as direct methanation of CO_2 [129], intermediates of both CO and formic acid, etc.

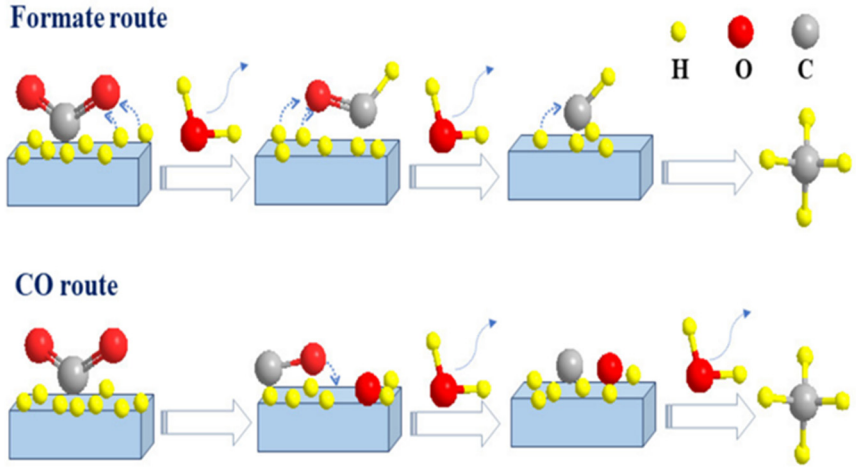


Figure 17. Different CO_2 methanation routes: formic acid route and CO route [68]. Copyright (2022) Catalysts.

5.1. CO Intermediate Mechanism

The CO pathway dissociates CO_2 from CO prior to methanation, and in the subsequent reaction, CO is converted to CH_4 by reacting with H_2 [68]. Although the H-assisted CO dissociation mechanism has been widely elucidated, there are differences in C–O bond breaking. Through DFT calculations and microdynamics studies, Li et al. [130] studied the cleavage of C–O bonds through CHO intermediates at low Co (0001) coverage, which mainly controls the methanation rate of CO. The mechanism is independent of the functional groups considered and the presence of graphitic carbon and may also be applicable to other Co surface structures, which may be used to design improved CO hydrogenation catalysts. Liu et al. [131] used the DFT calculation method to determine the internal reaction mechanism of CO_2 methanation on Ni/CeO_2 catalysts. It was found that CO_2 methanation on Ni/CeO_2 catalysts may be the conversion of CO_2 to CO by the RWGS, which then converts it to CH_4 through the same pathway as CO methanation. Because of the high energy barrier, there is no obvious advantage to forming formates or directly cracking C–O bonds. $CO_2* \rightarrow HOCO* \rightarrow CO* \rightarrow HCO* \rightarrow H_2CO* \rightarrow CH_2* \rightarrow CH_3* \rightarrow CH_4*$ is the optimal reaction pathway. C–O bond breaking of H-assisted H_2CO* is the rate-limiting step in the RWGS + CO-hydro pathway and plays a crucial role in the CO_2 methanation process. Bentrup et al. [132] studied the hydrogenation of CO_2 to CH_4 using Ni-sepiolite and Ni-marble as catalysts. On the Ni-sepiolite catalyst, the support material cannot adsorb CO_2,

and the dissociation adsorption of CO_2 in the presence of H_2 is observed to be activated by the dissociation of H atoms on NiO particles. Therefore, linear and bridged CO on NiO are identified as intermediates, where preferentially linearly bonded CO is hydrogenated to CH_4. Henriques et al. [133] performed multiple infrared measurements of zeolitride under CO_2/Ar or CO_2/H_2/Ar conditions. In the absence of H_2, CO_2 is almost not adsorbed by acidic zeolites, but in the presence of H_2, formates and carbonyl groups can be detected. The results show that the CO_2 methanation pathway is not formed by carbonate but by the dissociation of formate on Ni, forming adsorbed CO. Moreover, the results obtained using FTIR show the presence of bidentate carbonates on Ni^{2+} in the remaining NiO, which are highly thermally stable, and these bulk carbonates appear to be "spectator" species that do not participate in the methanation reaction. Therefore, CO is considered to be the main intermediate, and its dissociation is the determining step of CO_2 methanation. Similarly, Peebles et al. [134] investigated the methanation and dissociation of CO_2 on Ni (100) surfaces. The formation and activation energies of CH_4 and CO are 88.7 kJ·mol^{-1} and 72.8~82.4 kJ·mol^{-1}, respectively. Under the same reaction conditions, the activation energy and reaction rate of CO_2 to CH_4 are very close to the activation energy and reaction rate of CO methanation, so CO is an intermediate of CO_2 methanation [134]. Jacquemin et al. [135] studied the reaction mechanism of CO_2 methanation on an Rh/γ-Al_2O_3 catalyst. CH_4 is the only hydrocarbon product observed in MS. They think that CO_2 dissociates the CO, and oxygen adsorbs on the surface of the catalyst. In situ FTIR experiments demonstrated that the formation of CO (ads) is confirmed by linear RH-CO (2048 cm^{-1}), Rh^{3+}-CO (2123 cm^{-1}), and GEM-dicarbonyl Rh-$(CO)_2$ (2024 and 2092 cm^{-1}), and CO_2 with dicarbonyl and CO associated with Rh_2O_3 react most actively with hydrogen.

5.2. Mechanism of Formic Acid Intermediates

Muroyama et al. [136] studied the mechanism of CO_2 methanation on Ni/Al_2O_3 and Ni/Y_2O_3 catalysts using in situ FTIR spectroscopy. For Ni/Al_2O_3, CO_2 is dissociated and adsorbed on Ni particles. By introducing hydrogen into the atmosphere, linear and bridged CO adsorbents are converted to nickel carbonyl hydride or formyl substances, which are then hydrogenated into CH_4. Compared with Ni/Al_2O_3, formic acid and bridging CO are formed on Y_2O_3 support and Ni particles, respectively, and the reaction on Ni/Y_2O_3 is mainly carried out by forming formic acid adsorption. The CO adsorbates over the Ni particle are hydrogenated to CH_4 via the formation of nickel carbonyl hydride and/or formyl species. The hydroxyl group of Y_2O_3 facilitates the conversion of carbonates and bicarbonates into formates, and formic acid intermediates are located on Y_2O_3, so Ni and Y_2O_3 can directly participate in the reaction to make the catalyst more active overall [137].

Wang et al. [138] investigated the active site-dependent mechanism of CO_2 methanation catalyzed by the Ru/CeO_2 catalyst, using XANES, IR, and Raman to study the formation process of Ce^{3+}, surface hydroxyl, and oxygen vacancy in Ru/CeO_2, and clearly revealed their structural evolution under reaction conditions. Steady-state isotope transient kinetic analysis (SSITKA) type in situ drift infrared spectroscopy confirmed that in the presence of Ru/CeO_2, these substances are involved in the catalytic process of the formic acid route, and oxygen positions catalyze the dissociation of formic acid to methanol, which is the rate-determining step, and eventually form methane (as shown in Figure 18).

Wang et al. [126] studied the adsorption and methanation of CO_2 on an Ni/$Ce_{0.5}Zr_{0.5}O_2$ catalyst by in situ FTIR spectroscopy. They found that CO_2 is more likely to be adsorbed at the surface oxygen site near Ce(III), and the unidentate carbonates formed on Ce(III) are easy to hydrogenate. Formate is the main intermediate product in the reaction, which is formed by the hydrogenation of hydrogen carbonate and unidentate carbonates. Schild et al. [139] studied CO_2 methanation on an Ni-Zr catalyst by in situ FTIR. It was observed that CH_4 production increased with the depletion of the formic acid signal, and it was concluded that formate is a necessary intermediate for methane production.

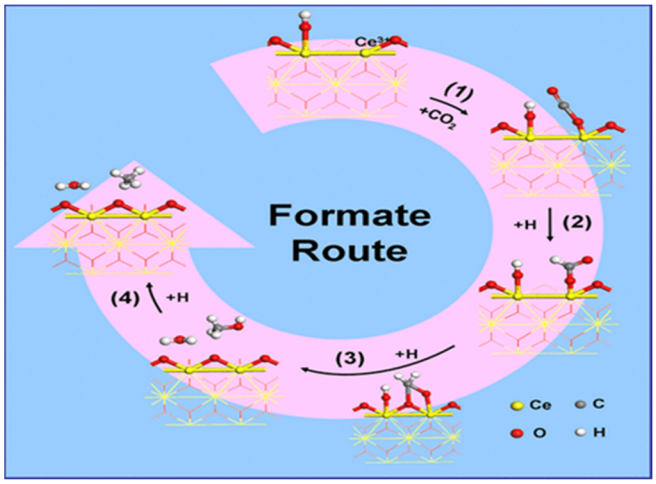


Figure 18. Schematic diagram of CO_2 methanated formic acid on Ru/CeO_2 catalyst [138]. Copyright (2016) Journal of the American Chemical Society.

6. Conclusions and Outlook

Non-noble metal catalysts have excellent catalytic activity for CO_2 methanation, are low priced, and are conducive to wide application in industry. Therefore, this paper reviews the latest progress of non-noble metal catalysts in CO_2 methanation from four aspects, namely CO_2 methanation thermodynamics and kinetics, non-noble metal catalysts, the effect of reaction conditions, and reaction mechanisms. In this work, the kinetics and thermodynamic characteristics of CO_2 methanation are explained, and it is clear that the reaction is an exothermic and volumetric shrinkage reaction, so low temperature and high pressure are more conducive to the reaction. Secondly, the influences of supports, promoters, and preparation methods on the catalytic performance of CO_2 methanation of Ni-based, Co-based, and other catalysts were summarized. It is found that the catalytic performance is affected mainly by reducing the particle size of the active metal, increasing the dispersion of the active metal, improving the strong metal–support interaction, and regulating the number of oxygen vacancies and the number of basic sites. In addition, the reaction conditions also affect the catalytic activity; suitable reaction conditions are beneficial to improving catalytic performance. We also discuss the reaction mechanism of CO_2 methanation and find that there are roughly three pathways, namely the CO pathway, the formate pathway, and the direct hydrogenation of CO_2 to CH_4. Based on this discussion, we suggest that the resistance to carbon accumulation and sulfur poisoning should be taken into account when improving the performance of the catalyst. Moreover, it is necessary to try more new materials and preparation methods, consider the effect of support morphology on catalyst performance, and use bimetallic catalysts with better performance.

Author Contributions: Conceptualization, Y.C. and S.H.; formal analysis, Y.C., S.H. and J.Y.; investigation, Y.C., S.H. and J.Y.; resources, K.H., X.C., L.X. and C.D.; data curation, C.L. and S.P.; writing—original draft preparation, Y.C., S.H. and J.Y.; writing—review and editing, K.H., X.C., L.X. and C.D.; project administration, R.G. and C.Z.; funding acquisition, R.G. and C.Z. All authors have read and agreed to the published version of the manuscript.

Funding: This work was funded by "Carbon Upcycling Project for Platform Chemicals" (Project Nos. 2022M3J3A1045999, 2022M3J3A1039377) through the National Research Foundation (NRF) funded by the Ministry of Science and ICT, Republic of Korea. We also supported by the Natural Science Foundation of Jiangsu Province (Grant Nos. BZ2023051, BK20200694, 20KJB530002, and 21KJB480014), the Jiangsu Specially-Appointed Professors Program, and Jiangsu Province Innovation and Entrepreneurship Training Program for College Students (Grant No. 202310291239Y).

Conflicts of Interest: The authors declare no conflict of interest.

References

1. Wilberforce, T.; Olabi, A.G.; Sayed, E.T.; Elsaid, K.; Abdelkareem, M.A. Progress in carbon capture technologies. *Sci. Total Environ.* **2021**, *761*, 143203. [CrossRef] [PubMed]
2. Mora, C.; Spirandelli, D.; Franklin, E.C.; Lynham, J.; Kantar, M.B.; Miles, W.; Smith, C.Z.; Freel, K.; Moy, J.; Louis, L.V.; et al. Broad threat to humanity from cumulative climate hazards intensified by greenhouse gas emissions. *Nat. Clim. Change* **2018**, *8*, 1062–1071. [CrossRef]
3. Rogelj, J.; Geden, O.; Cowie, A.; Reisinger, A. Three ways to improve net-zero emissions targets. *Nature* **2021**, *591*, 365–368. [CrossRef] [PubMed]
4. Roelfsema, M.; van Soest, H.L.; Harmsen, M.; van Vuuren, D.P.; Bertram, C.; den Elzen, M.; Höhne, N.; Iacobuta, G.; Krey, V.; Kriegler, E.; et al. Taking stock of national climate policies to evaluate implementation of the Paris Agreement. *Nat. Commun.* **2020**, *11*, 2096. [CrossRef]
5. Ishaq, H.; Dincer, I.; Crawford, C. A review on hydrogen production and utilization: Challenges and opportunities. *Int. J. Hydrogen Energy* **2022**, *47*, 26238–26264. [CrossRef]
6. Lu, P.; Chang, X.N.; Yu, W.J.; Hu, Q.W.; Ali, K.M.; Xing, C.; Du, C.; Yang, Z.X.; Chen, S.Y. Synergistic effects of ZnO-ZrO_2@SAPO-34 core-shell catalyst in catalyzing CO_2 hydrogenation for the synthesis of light olefins. *Renew. Energy* **2023**, *209*, 546–557. [CrossRef]
7. Roy, S.C.; Varghese, O.K.; Paulose, M.; Grimes, C.A. Toward Solar Fuels: Photocatalytic Conversion of Carbon Dioxide to Hydrocarbons. *ACS Nano* **2010**, *4*, 1259–1278. [CrossRef]
8. Zhou, Z.X.; Gao, P. Direct carbon dioxide hydrogenation to produce bulk chemicals and liquid fuels via heterogeneous catalysis. *Chin. J. Catal.* **2022**, *43*, 2045–2056. [CrossRef]
9. Zhang, Z.E.; Pan, S.Y.; Li, H.; Cai, J.C.; Olabi, A.G.; Anthony, E.J.; Manovic, V. Recent advances in carbon dioxide utilization. *Renew. Sustain. Energy Rev.* **2020**, *125*, 109799. [CrossRef]
10. Wang, H.Q. Nanostructure@metal-organic frameworks (MOFs) for catalytic carbon dioxide (CO_2) conversion in photocatalysis, electrocatalysis, and thermal catalysis. *Nano Res.* **2022**, *15*, 2834–2854. [CrossRef]
11. Fan, W.K.; Tahir, M. Current Trends and Approaches to Boost the Performance of Metal Organic Frameworks for Carbon Dioxide Methanation through Photo/Thermal Hydrogenation: A Review. *Ind. Eng. Chem. Res.* **2021**, *60*, 13149–13179. [CrossRef]
12. Gao, P.; Zhong, L.S.; Han, B.X.; He, M.Y.; Sun, Y.H. Green Carbon Science: Keeping the Pace in Practice. *Angew. Chem. Int. Ed.* **2022**, *61*, e202210095. [CrossRef] [PubMed]
13. Saeidi, S.; Najari, S.; Hessel, V.; Wilson, K.; Keil, F.J.; Concepcion, P.; Suib, S.L.; Rodrigues, A.E. Recent advances in CO_2 hydrogenation to value-added products—Current challenges and future directions. *Prog. Energy Combust. Sci.* **2021**, *85*, 100905. [CrossRef]
14. Braga, A.H.; Vidinha, P.; Rossi, L.M. Hydrogenation of carbon dioxide: From waste to value. *Curr. Opin. Green Sustain. Chem.* **2020**, *26*, 100386. [CrossRef]
15. Saravanan, A.; Kumar, P.S.; Vo, D.V.N.; Jeevanantham, S.; Bhuvaneswari, V.; Narayanan, V.A.; Yaashikaa, P.R.; Swetha, S.; Reshma, B. A comprehensive review on different approaches for CO_2 utilization and conversion pathways. *Chem. Eng. Sci.* **2021**, *236*, 116515. [CrossRef]
16. Chang, X.N.; Hondo, E.; Yu, W.J.; Ali, K.M.; Nyako, A.; Xing, C.; Yang, Z.X.; Lu, P. Effect of acidity and oxygen vacancy in Mn loaded SAPO-34 on CO_2 hydrogenation to light olefin. *Fuel* **2023**, *353*, 129160. [CrossRef]
17. Wang, W.Y.; Zhou, W.; Tang, Y.C.; Cao, W.C.; Docherty, S.R.; Wu, F.W.; Cheng, K.; Zhang, Q.H.; Coperet, C.; Wang, Y. Selective Oxidation of Methane to Methanol over Au/H-MOR. *J. Am. Chem. Soc.* **2023**, *145*, 12928–12934. [CrossRef]
18. Karakaya, C.; Kee, R.J. Progress in the direct catalytic conversion of methane to fuels and chemicals. *Prog. Energy Combust. Sci.* **2016**, *55*, 60–97. [CrossRef]
19. Ghaib, K.; Nitz, K.; Ben-Fares, F.Z. Catalytic Methanation of Carbon Dioxide. *Chem. Ing. Tech.* **2016**, *88*, 1435–1443. [CrossRef]
20. Fan, W.K.; Tahir, M. Recent trends in developments of active metals and heterogenous materials for catalytic CO_2 hydrogenation to renewable methane: A review. *J. Environ. Chem. Eng.* **2021**, *9*, 105460. [CrossRef]
21. El Sibai, A.; Struckmann, L.K.R.; Sundmacher, K. Model-based Optimal Sabatier Reactor Design for Power-to-Gas Applications. *Energy Technol.* **2017**, *5*, 911–921. [CrossRef]
22. Vogt, C.; Monai, M.; Kramer, G.J.; Weckhuysen, B.M. The renaissance of the Sabatier reaction and its applications on Earth and in space. *Nat. Catal.* **2019**, *2*, 188–197. [CrossRef]
23. Ghaib, K.; Nitz, K.; Ben-Fares, F.Z. Chemical methanation of CO_2: A review. *ChemBioEng Rev.* **2016**, *3*, 266–275. [CrossRef]
24. Jo, S.B.; Woo, J.H.; Lee, J.H.; Kim, T.Y.; Kang, H.I.; Lee, S.C.; Kim, J.C. CO_2 green technologies in CO_2 capture and direct utilization processes: Methanation, reverse water-gas shift, and dry reforming of methane. *Sustain. Energy Fuels* **2020**, *4*, 5543–5549. [CrossRef]
25. Frontera, P.; Macario, A.; Ferraro, M.; Antonucci, P. Supported Catalysts for CO_2 Methanation: A Review. *Catalysts* **2017**, *7*, 59. [CrossRef]
26. Ekeoma, B.C.; Yusuf, M.; Johari, K.; Abdullah, B. Mesoporous silica supported Ni-based catalysts for methane dry reforming: A review of recent studies. *Int. J. Hydrogen Energy* **2022**, *47*, 41596–41620. [CrossRef]
27. Alrafei, B.; Polaert, I.; Ledoux, A.; Azzolina-Jury, F. Remarkably stable and efficient Ni and Ni-Co catalysts for CO_2 methanation. *Catal. Today* **2020**, *346*, 23–33. [CrossRef]

28. Jia, X.Y.; Zhang, X.S.; Rui, N.; Hu, X.; Liu, C.J. Structural effect of Ni/ZrO_2 catalyst on CO_2 methanation with enhanced activity. *Appl. Catal. B Environ.* **2019**, *244*, 159–169. [CrossRef]
29. Tan, C.H.; Nomanbhay, S.; Shamsuddin, A.; Park, Y.K.; Hernandez-Cocoletzi, H.; Show, P.L. Current Developments in Catalytic Methanation of Carbon Dioxide—A Review. *Front. Energy Res.* **2022**, *9*, 795423. [CrossRef]
30. Debek, R.; Azzolina-Jury, F.; Travert, A.; Mauge, F. A review on plasma-catalytic methanation of carbon dioxide—Looking for an efficient catalyst. *Renew. Sustain. Energy Rev.* **2019**, *116*, 109427. [CrossRef]
31. Fan, T.; Liu, H.L.; Shao, S.X.; Gong, Y.J.; Li, G.D.; Tang, Z.Y. Cobalt Catalysts Enable Selective Hydrogenation of CO_2 toward Diverse Products: Recent Progress and Perspective. *J. Phys. Chem. Lett.* **2021**, *12*, 10486–10496. [CrossRef] [PubMed]
32. Malhi, H.S.; Zhang, Z.Z.; Shi, Y.L.; Gao, X.H.; Liu, W.Q.; Tu, W.F.; Han, Y.F. The promotional effects of carbon nanotube on Fe_5C_2-ZnO catalysts for CO_2 hydrogenation to heavy olefins. *Fuel* **2023**, *339*, 127267. [CrossRef]
33. Guo, X.Y.; Liu, B.; Gao, X.H.; He, F.G.; Ma, Q.X.; Fan, S.B.; Zhao, T.S.; Tian, J.M.; Reubroycharoen, P.; Zhang, J.L. Improved olefin selectivity during CO hydrogenation on hydrophilic Fe/HAP catalysts. *Catal. Today* **2023**, *410*, 193–204. [CrossRef]
34. Li, Z.; Qu, J.; Wang, W.; Wang, B.; Ma, X. Effect of CO_2 in syngas on methanation performance of Mo-based catalyst. *J. Fuel Chem. Technol.* **2016**, *44*, 985–992.
35. Quindimil, A.; De-La-Torre, U.; Pereda-Ayo, B.; Davo-Quinonero, A.; Bailon-Garcia, E.; Lozano-Castello, D.; Gonzalez-Marcos, J.A.; Bueno-Lopez, A.; Gonzalez-Velasco, J.R. Effect of metal loading on the CO_2 methanation: A comparison between alumina supported Ni and Ru catalysts. *Catal. Today* **2020**, *356*, 419–432. [CrossRef]
36. Italiano, C.; Llorca, J.; Pino, L.; Ferraro, M.; Antonucci, V.; Vita, A. CO and CO_2 methanation over Ni catalysts supported on CeO_2, Al_2O_3 and Y_2O_3 oxides. *Appl. Catal. B Environ.* **2020**, *264*, 118494. [CrossRef]
37. Gac, W.; Zawadzki, W.; Rotko, M.; Greluk, M.; Slowik, G.; Kolb, G. Effects of support composition on the performance of nickel catalysts in CO_2 methanation reaction. *Catal. Today* **2020**, *357*, 468–482. [CrossRef]
38. Wang, K.; Men, Y.; Liu, S.; Wang, J.G.; Li, Y.Y.; Tang, Y.H.; Li, Z.P.; An, W.; Pan, X.L.; Li, L. Decoupling the size and support/metal loadings effect of Ni/SiO_2 catalysts for CO_2 methanation. *Fuel* **2021**, *304*, 121388. [CrossRef]
39. Iglesias, I.; Quindimil, A.; Marino, F.; De-La-Torre, U.; Gonzalez-Velasco, J.R. Zr promotion effect in CO_2 methanation over ceria supported nickel catalysts. *Int. J. Hydrogen Energy* **2019**, *44*, 1710–1719. [CrossRef]
40. Wang, X.L.; Zhu, L.J.; Zhuo, Y.X.; Zhu, Y.Q.; Wang, S.R. Enhancement of CO_2 Methanation over La-Modified Ni/SBA-15 Catalysts Prepared by Different Doping Methods. *ACS Sustain. Chem. Eng.* **2019**, *7*, 14647–14660. [CrossRef]
41. Huynh, H.L.; Zhu, J.; Zhang, G.H.; Shen, Y.L.; Tucho, W.M.; Ding, Y.; Yu, Z.X. Promoting effect of Fe on supported Ni catalysts in CO_2 methanation by in situ DRIFTS and DFT study. *J. Catal.* **2020**, *392*, 266–277. [CrossRef]
42. Pham, C.Q.; Bahari, M.B.; Kumar, P.S.; Ahmed, S.F.; Xiao, L.L.; Kumar, S.; Qazaq, A.S.; Siang, T.J.; Tran, H.T.; Islam, A.; et al. Carbon dioxide methanation on heterogeneous catalysts: A review. *Environ. Chem. Lett.* **2022**, *20*, 3613–3630. [CrossRef]
43. Baamran, K.S.; Tahir, M. Thermodynamic investigation and experimental analysis on phenol steam reforming towards enhanced H-2 production over structured Ni/$ZnTiO_3$ nanocatalyst. *Energy Convers. Manag.* **2019**, *180*, 796–810. [CrossRef]
44. Gao, J.J.; Wang, Y.L.; Ping, Y.; Hu, D.C.; Xu, G.W.; Gu, F.N.; Su, F.B. A thermodynamic analysis of methanation reactions of carbon oxides for the production of synthetic natural gas. *RSC Adv.* **2012**, *2*, 2358–2368. [CrossRef]
45. Massa, F.; Coppola, A.; Scala, F. A thermodynamic study of sorption-enhanced CO_2 methanation at low pressure. *J. CO_2 Util.* **2020**, *35*, 176–184. [CrossRef]
46. Champon, I.; Bengaouer, A.; Chaise, A.; Thomas, S.; Roger, A.C. Carbon dioxide methanation kinetic model on a commercial Ni/Al_2O_3 catalyst. *J. CO_2 Util.* **2019**, *34*, 256–265. [CrossRef]
47. Hussain, I.; Jalil, A.A.; Hassan, N.S.; Hamid, M.Y.S. Recent advances in catalytic systems for CO_2 conversion to substitute natural gas (SNG): Perspective and challenges. *J. Energy Chem.* **2021**, *62*, 377–407. [CrossRef]
48. Ashok, J.; Pati, S.; Hongmanorom, P.; Tianxi, Z.; Junmei, C.; Kawi, S. A review of recent catalyst advances in CO_2 methanation processes. *Catal. Today* **2020**, *356*, 471–489.
49. Lee, W.J.; Li, C.; Prajitno, H.; Yoo, J.; Patel, J.; Yang, Y.; Lim, S. Recent trend in thermal catalytic low temperature CO_2 methanation: A critical review. *Catal. Today* **2021**, *368*, 2–19. [CrossRef]
50. Fan, W.K.; Tahir, M. Investigating the product distribution behaviour of CO_2 methanation through thermodynamic optimized experimental approach using micro/nano structured titania catalyst. *Energy Convers. Manag.* **2022**, *254*, 115240. [CrossRef]
51. González-Castaño, M.; González-Arias, J.; Bobadilla, L.F.; Ruíz-López, E.; Odriozola, J.A.; Arellano-García, H. In-situ DRIFTS steady-state study of CO_2 and CO methanation over Ni-promoted catalysts. *Fuel* **2023**, *338*, 127241. [CrossRef]
52. Mutz, B.; Sprenger, P.; Wang, W.; Wang, D.; Kleist, W.; Grunwaldt, J.-D. Operando Raman spectroscopy on CO_2 methanation over alumina-supported Ni, Ni_3Fe and $NiRh_{0.1}$ catalysts: Role of carbon formation as possible deactivation pathway. *Appl. Catal. A Gen.* **2018**, *556*, 160–171. [CrossRef]
53. Zhu, M.; Tian, P.; Cao, X.; Chen, J.; Pu, T.; Shi, B.; Xu, J.; Moon, J.; Wu, Z.; Han, Y.-F. Vacancy engineering of the nickel-based catalysts for enhanced CO_2 methanation. *Appl. Catal. B Environ.* **2021**, *282*, 119561. [CrossRef]
54. Ma, L.; Ye, R.; Huang, Y.; Reina, T.R.; Wang, X.; Li, C.; Zhang, X.L.; Fan, M.; Zhang, R.; Liu, J. Enhanced low-temperature CO_2 methanation performance of Ni/ZrO_2 catalysts via a phase engineering strategy. *Chem. Eng. J.* **2022**, *446*, 137031. [CrossRef]
55. Ahmad, W.; Al-Matar, A.; Shawabkeh, R.; Rana, A. An experimental and thermodynamic study for conversion of CO_2 to CO and methane over Cu-K/Al_2O_3. *J. Environ. Chem. Eng.* **2016**, *4*, 2725–2735. [CrossRef]

56. Yarbaş, T.; Ayas, N. A detailed thermodynamic analysis of CO_2 hydrogenation to produce methane at low pressure. *Int. J. Hydrogen Energy* **2024**, *49*, 1134–1144. [CrossRef]
57. Hussain, I.; Jalil, A.A.; Izan, S.M.; Azami, M.S.; Kidam, K.; Ainirazali, N.; Ripin, A. Thermodynamic and experimental explorations of CO_2 methanation over highly active metal-free fibrous silica-beta zeolite (FS@SiO_2-BEA) of innovative morphology. *Chem. Eng. Sci.* **2021**, *229*, 116015. [CrossRef]
58. Mihet, M.; Grad, O.; Blanita, G.; Radu, T.; Lazar, M.D. Effective encapsulation of Ni nanoparticles in metal-organic frameworks and their application for CO_2 methanation. *Int. J. Hydrogen Energy* **2019**, *44*, 13383–13396. [CrossRef]
59. McLain, J.E.T.; Kepler, T.B.; Ahmann, D.M. Belowground factors mediating changes in methane consumption in a forest soil under elevated CO_2. *Glob. Biogeochem. Cycle* **2002**, *16*, 23-1-23-14. [CrossRef]
60. Jaffar, M.M.; Nahil, M.A.; Williams, P.T. Parametric Study of CO_2 Methanation for synthetic nature gas production. *Energy Technol.* **2019**, *7*, 1900795. [CrossRef]
61. Aziz, M.A.A.; Jalil, A.A.; Triwahyono, S.; Mukti, R.R.; Taufiq-Yap, Y.H.; Sazegar, M.R. Highly active Ni-promoted mesostructured silica nanoparticles for CO_2 methanation. *Appl. Catal. B Environ.* **2014**, *147*, 359–368. [CrossRef]
62. Moghaddam, S.V.; Rezaei, M.; Meshkani, F.; Daroughegi, R. Synthesis of nanocrystalline mesoporous Ni/$Al_2O_3SiO_2$ catalysts for CO_2 methanation reaction. *Int. J. Hydrogen Energy* **2018**, *43*, 19038–19046.
63. Nguyen, N.-P.; Le, B.-N.T.; Nguyen, T.; Dinh, M.T.N.; Nguyen, H.-H.T.; Vo, D.-V.N.; Duy, N.P.T.; Nguyen, H.-D.P.; Pham, T.-P.T. Fabrication of the coke-resistant and easily reducible Ni/SiC catalyst for CO_2 methanation. *J. Energy Inst.* **2023**, *110*, 101332. [CrossRef]
64. Ridzuan, N.D.M.; Shaharun, M.S.; Anawar, M.A.; Ud-Din, I. Ni-Based Catalyst for Carbon Dioxide Methanation: A Review on Performance and Progress. *Catalysts* **2022**, *12*, 469. [CrossRef]
65. Wu, J.; Gao, J.; Lian, S.; Li, J.; Sun, K.; Zhao, S.; Kim, Y.D.; Ren, Y.; Zhang, M.; Liu, Q.; et al. Engineering the oxygen vacancies enables Ni single-atom catalyst for stable and efficient C-H activation. *Appl. Catal. B Environ.* **2022**, *314*, 121516. [CrossRef]
66. Namvar, F.; Salavati-Niasari, M.; Meshkani, F. Effect of the Rare Earth Metals (Tb, Nd, Dy) addition for the modification of nickel catalysts supported on alumina in CO_2 Methanation. *Int. J. Hydrogen Energy* **2023**, *48*, 1877–1891. [CrossRef]
67. Shen, L.; Xu, J.; Zhu, M.; Han, Y.-F. Essential Role of the Support for Nickel-Based CO_2 Methanation Catalysts. *ACS Catal.* **2020**, *10*, 14581–14591. [CrossRef]
68. Li, L.; Zeng, W.Q.; Song, M.X.; Wu, X.S.; Li, G.Y.; Hu, C.W. Research Progress and Reaction Mechanism of CO_2 Methanation over Ni-Based Catalysts at Low Temperature: A Review. *Catalysts* **2022**, *12*, 244. [CrossRef]
69. Schreiter, N.; Kirchner, J.; Kureti, S. A DRIFTS and TPD study on the methanation of CO_2 on Ni/Al_2O_3 catalyst. *Catal. Commun.* **2020**, *140*, 105988. [CrossRef]
70. Chen, Y.M.; Hou, Z.G.; Wang, C.; Ma, X.; Yang, H.; Wang, W.; Zhou, L.; Zhang, Y. An Active Manganese Promoted Ni/Al_2O_3 Catalyst for Low Temperature CO_2 Methanation. *Catal. Lett.* **2023**. [CrossRef]
71. Cherevotan, A.; Ray, B.; Churipard, S.R.; Kaur, K.; Gautam, U.K.; Vinod, C.P.; Peter, S.C. Influence of support textural property on CO_2 to methane activity of Ni/SiO_2 catalysts. *Appl. Catal. B Environ.* **2022**, *317*, 121692. [CrossRef]
72. Xu, L.L.; Xu, C.Y.; Chen, B.; Bian, Y.F.; Wen, X.Y.; Cheng, G.; Wu, C.E.; Qiu, J.; Chen, M.D. One-pot synthesis of hexagonal mesoporous silica confined Ni based catalysts with advanced CO_2 methanation performance. *Fuel* **2023**, *333*, 126411. [CrossRef]
73. Zhou, Z.; Li, X.Z.; Li, J.J.; You, Z.X. Promoting CO_2 methanation performance of Ru/$TiO_{(2)}$through Co-activity of exposing (001) facets and oxygen vacancies of TiO_2. *Mater. Sci. Semicond. Process.* **2022**, *146*, 106677. [CrossRef]
74. Unwiset, P.; Chanapattharapol, K.C.; Kidkhunthod, P.; Poo-arporn, Y.; Ohtani, B. Catalytic activities of titania-supported nickel for carbon-dioxide methanation. *Chem. Eng. Sci.* **2020**, *228*, 115955. [CrossRef]
75. Li, J.; Lin, Y.P.; Pan, X.L.; Miao, D.Y.; Ding, D.; Cui, Y.; Dong, J.H.; Bao, X.H. Enhanced CO_2 Methanation Activity of Ni/Anatase Catalyst by Tuning Strong Metal-Support Interactions. *ACS Catal.* **2019**, *9*, 6342–6348. [CrossRef]
76. Espino, O.E.E.; Zonetti, P.C.; Celin, R.R.; Costa, L.T.; Alves, O.C.; Spadotto, J.C.; Appel, L.G.; de Avillez, R.R. The tendency of supports to generate oxygen vacancies and the catalytic performance of Ni/ZrO_2 and Ni/Mg(Al)O in CO_2 methanation. *Catal. Sci. Technol.* **2022**, *12*, 1324–1338. [CrossRef]
77. He, Y.; Shen, H.D.; Bai, Y.H.; Niu, X.; Zhao, Y.K.; Wu, C.; Yang, S.W.; Cao, Y.L.; Zhang, Q.Y.; Zhang, H.P. Construction of the Low-Loading Ni/CeO_2 Catalyst with a Boosted CO_2 Methanation Performance via the Facile Pyrolysis CeO_2 Support. *Ind. Eng. Chem. Res.* **2022**, *61*, 15948–15960. [CrossRef]
78. Bian, Y.F.; Xu, C.Y.; Wen, X.Y.; Xu, L.L.; Cui, Y.; Wang, S.H.; Wu, C.E.; Qiu, J.; Cheng, G.; Chen, M.D. CO_2 methanation over the Ni-based catalysts supported on nano-CeO_2 with varied morphologies. *Fuel* **2023**, *331*, 125755. [CrossRef]
79. Li, B.; Wang, F.; Li, K.; Ning, P.; Chen, M.; Zhang, C. CeO_2-supported Fe, Co and Ni toward CO_2 hydrogenation: Tuning catalytic performance via metal-support interaction. *J. Rare Earths* **2023**, *41*, 926–932. [CrossRef]
80. Zhang, Z.; Ding, H.; Pan, W.; Ma, J.; Zhang, K.; Zhao, Y.; Song, J.; Wei, C.; Lin, F. Research progress of Metal-Organic Frameworks (MOFs) for CO_2 Conversion in CCUS. *J. Energy Inst.* **2023**, *108*, 101226. [CrossRef]
81. Li, Y.-T.; Zhou, L.; Cui, W.-G.; Li, Z.-F.; Li, W.; Hu, T.L. Iron promoted MOF-derived carbon encapsulated NiFe alloy nanoparticles core-shell catalyst for CO_2 methanation. *J. CO2 Util.* **2022**, *62*, 102093. [CrossRef]
82. Karam, L.; Bacariza, M.C.; Lopes, J.M.; Henriques, C.; Reboul, J.; El Hassan, N.; Massiani, P. Mesoporous nickel-alumina catalysts derived from MIL-53(Al) metal-organic framework: A new promising path for synthesizing CO_2 methanation catalysts. *J. CO2 Util.* **2021**, *51*, 101651. [CrossRef]

83. Feng, X.; Wang, K.; Zhou, M.; Li, F.; Liu, J.; Zhao, M.; Zhao, L.; Song, X.; Zhang, P.; Gao, L. Metal organic framework derived Ni/CeO_2 catalyst with highly dispersed ultra-fine Ni nanoparticles: Impregnation synthesis and the application in CO_2 methanation. *Ceram. Int.* **2021**, *47*, 12366–12374. [CrossRef]
84. Zhang, Z.H.; Feng, K.; Yan, B.H. Enhanced Ni-Ce interactions to enable efficient low-temperature catalytic CO_2 methanation. *Catal. Sci. Technol.* **2022**, *12*, 4698–4708. [CrossRef]
85. Moghaddam, S.V.; Rezaei, M.; Meshkani, F. Surfactant-Free Sol-Gel Synthesis Method for the Preparation of Mesoporous High Surface Area NiO-Al_2O_3 Nanopowder and Its Application in Catalytic CO_2 Methanation. *Energy Technol.* **2020**, *8*, 1900778. [CrossRef]
86. Liu, X.D.; Zhang, L.J.; Li, Z.H. Promotion Effect of TiO_2 on Ni/SiO_2 Catalysts Prepared by Hydrothermal Method for CO_2 Methanation. *Energy Technol.* **2023**, *11*, 2201526. [CrossRef]
87. Zhang, Y.F.; Zhang, G.J.; Liu, J.; Li, T.S.; Zhang, X.D.; Wang, Y.; Zhao, Y.Q.; Li, G.Q.; Zhang, Y.F. Insight into the role of preparation method on the structure and size effect of Ni/MSS catalysts for dry reforming of methane. *Fuel Process. Technol.* **2023**, *250*, 107891. [CrossRef]
88. Yan, P.H.; Mensah, J.; Adesina, A.; Kennedy, E.; Stockenhuber, M. Highly-dispersed Ni on BEA catalyst prepared by ion-exchange-deposition-precipitation for improved hydrodeoxygenation activity. *Appl. Catal. B Environ.* **2020**, *267*, 118690. [CrossRef]
89. Tsiotsias, A.I.; Charisiou, N.D.; Yentekakis, I.V.; Goula, M.A. Bimetallic Ni-Based Catalysts for CO_2 Methanation: A Review. *Nanomaterials* **2020**, *11*, 28. [CrossRef]
90. Liu, K.; Xu, X.; Xu, J.; Fang, X.; Liu, L.; Wang, X. The distributions of alkaline earth metal oxides and their promotional effects on Ni/CeO_2 for CO_2 methanation. *J. CO_2 Util.* **2020**, *38*, 113–124. [CrossRef]
91. Shirsath, A.B.; Schulte, M.L.; Kreitz, B.; Tischer, S.; Grunwaldt, J.D.; Deutschmann, O. Spatially-resolved investigation of CO_2 methanation over Ni/γ-Al_2O_3 and $Ni_{3.2}Fe/\gamma$-Al_2O_3 catalysts in a packed-bed reactor. *Chem. Eng. J.* **2023**, *469*, 143847. [CrossRef]
92. Shafiee, P.; Alavi, S.M.; Rezaei, M. Solid-state synthesis method for the preparation of cobalt doped Ni-Al_2O_3 mesoporous catalysts for CO_2 methanation. *Int. J. Hydrogen Energy* **2021**, *46*, 3933–3944. [CrossRef]
93. Daroughegi, R.; Meshkani, F.; Rezaei, M. Enhanced low-temperature activity of CO_2 methanation over ceria-promoted Ni-Al_2O_3 nanocatalyst. *Chem. Eng. Sci.* **2021**, *230*, 116194. [CrossRef]
94. Li, W.H.; Zhang, G.H.; Jiang, X.; Liu, Y.; Zhu, J.; Ding, F.S.; Liu, Z.M.; Guo, X.W.; Song, C.S. CO_2 Hydrogenation on Unpromoted and M-Promoted Co/TiO_2 Catalysts (M = Zr, K, Cs): Effects of Crystal Phase of Supports and Metal-Support Interaction on Tuning Product Distribution. *ACS Catal.* **2019**, *9*, 2739–2751. [CrossRef]
95. Li, W.H.; Liu, Y.; Mu, M.C.; Ding, F.S.; Liu, Z.M.; Guo, X.W.; Song, C.S. Organic acid-assisted preparation of highly dispersed Co/ZrO_2 catalysts with superior activity for CO_2 methanation. *Appl. Catal. B Environ.* **2019**, *254*, 531–540. [CrossRef]
96. Li, W.; Nie, X.; Jiang, X.; Zhang, A.; Ding, F.; Liu, M.; Liu, Z.; Guo, X.; Song, C. ZrO_2 support imparts superior activity and stability of Co catalysts for CO_2 methanation. *Appl. Catal. B Environ.* **2018**, *220*, 397–408. [CrossRef]
97. Yu, W.Z.; Fu, X.P.; Xu, K.; Ling, C.; Wang, W.W.; Jia, C.J. CO_2 methanation catalyzed by a Fe-Co/Al_2O_3 catalyst. *J. Environ. Chem. Eng.* **2021**, *9*, 105594. [CrossRef]
98. Jimenez, J.D.; Wen, C.; Lauterbach, J. Design of highly active cobalt catalysts for CO_2 hydrogenation via the tailoring of surface orientation of nanostructures. *Catal. Sci. Technol.* **2019**, *9*, 1970–1978. [CrossRef]
99. Jimenez, J.; Bird, A.; Santiago, M.S.; Wen, C.; Lauterbach, J. Supported Cobalt Nanorod Catalysts for Carbon Dioxide Hydrogenation. *Energy Technol.* **2017**, *5*, 884–891. [CrossRef]
100. Gholampour, N.; Zhao, Y.R.; Devred, F.; Sassoye, C.; Casale, S.; Debecker, D.P. CO_2 Methanation over Cobalt Nanoparticles Embedded in ZIF-L-Derived Porous Carbon. *ChemCatChem* **2023**, *15*, e202201338. [CrossRef]
101. Liang, L.X.; Miao, C.; Ke, X.; Peng, Y.H.; Chen, G.; Ouyang, J. A superior strategy for CO_2 methanation under atmospheric pressure: Organic acid-assisted Co nanoparticles assembly on diatomite. *Fuel* **2023**, *351*, 128931. [CrossRef]
102. Efremova, A.; Rajkumar, T.; Szamosvolgyi, A.; Sapi, A.; Baan, K.; Szenti, I.; Gomez-Perez, J.; Varga, G.; Kiss, J.; Halasi, G.; et al. Complexity of a Co_3O_4 System under Ambient-Pressure CO_2 Methanation: Influence of Bulk and Surface Properties on the Catalytic Performance. *J. Phys. Chem. C* **2021**, *125*, 7130–7141. [CrossRef]
103. Nguyen, T.H.; Kim, H.B.; Park, E.D. CO and CO_2 Methanation over CeO_2-Supported Cobalt Catalysts. *Catalysts* **2022**, *12*, 212. [CrossRef]
104. Gassler, M.; Stahl, J.; Schowalter, M.; Pokhrel, S.; Rosenauer, A.; Madler, L.; Guttel, R. The Impact of Support Material of Cobalt-Based Catalysts Prepared by Double Flame Spray Pyrolysis on CO_2 Methanation Dynamics. *ChemCatChem* **2022**, *14*, e202200286. [CrossRef]
105. Stahl, J.; Ilsemann, J.; Pokhrel, S.; Schowalter, M.; Tessarek, C.; Rosenauer, A.; Eickhoff, M.; Baumer, M.; Madler, L. Comparing Co-catalytic Effects of ZrO_X, SmO_X, and Pt on CO_X Methanation over Co-based Catalysts Prepared by Double Flame Spray Pyrolysis. *ChemCatChem* **2021**, *13*, 2815–2831. [CrossRef]
106. Tu, J.H.; Wu, H.H.; Qian, Q.L.; Han, S.T.; Chu, M.G.; Jia, S.Q.; Feng, R.T.; Zhai, J.X.; He, M.Y.; Han, B.X. Low temperature methanation of CO_2 over an amorphous cobalt-based catalyst. *Chem. Sci.* **2021**, *12*, 3937–3943. [CrossRef] [PubMed]
107. Franken, T.; Terreni, J.; Borgschulte, A.; Heel, A. Solid solutions in reductive environment—A case study on improved CO_2 hydrogenation to methane on cobalt based catalysts derived from ternary mixed metal oxides by modified reducibility. *J. Catal.* **2020**, *382*, 385–394. [CrossRef]

108. Biswas, S.; Kundu, C.; Kulkarni, A.P.; Kattel, S.; Giddey, S.; Bhattacharya, S. A Study on CO_2 Hydrogenation Using a Ceria-Zirconia Mixed Oxide (Ce_xZr_1-xO_2)-Supported Fe Catalyst. *Ind. Eng. Chem. Res.* **2021**, *60*, 14410–14423. [CrossRef]
109. Kirchner, J.; Zambrzycki, C.; Kureti, S.; Guttel, R. CO_2 Methanation on Fe Catalysts Using Different Structural Concepts. *Chem. Ing. Tech.* **2020**, *92*, 603–607. [CrossRef]
110. Misra, A.; Zambrzycki, C.; Kloker, G.; Kotyrba, A.; Anjass, M.H.; Castillo, I.F.; Mitchell, S.G.; Guttel, R.; Streb, C. Water Purification and Microplastics Removal using Magnetic Polyoxometalate-Supported Ionic Liquid Phases (magPOM-SILPs). *Angew. Chem. Int. Ed.* **2020**, *59*, 1601–1605. [CrossRef]
111. Kalakkad, D.S.; Shroff, M.D.; Kohler, S.; Jackson, N.; Datye, A.K. Attrition of precipitated iron Fischer-Tropsch catalysts. *Appl. Catal. A Gen.* **1995**, *133*, 335–350. [CrossRef]
112. Iqbal, M.M.A.; Toemen, S.; Abu bakar, W.A.W.; Razak, F.I.A.; Rosid, S.J.M.; Azelee, N.I.W. Catalytic methanation over nanoparticle heterostructure of Ru/Fe/Ce/γ-Al_2O_3 catalyst: Performance and characterization. *Renew. Energy* **2020**, *162*, 513–524. [CrossRef]
113. Franken, T.; Heel, A. Are Fe based catalysts an upcoming alternative to Ni in CO_2 methanation at elevated pressure? *J. CO2 Util.* **2020**, *39*, 101175. [CrossRef]
114. Baysal, Z.; Kureti, S. CO_2 methanation on Mg-promoted Fe catalysts. *Appl. Catal. B Environ.* **2020**, *262*, 118300. [CrossRef]
115. Samanta, A.; Landau, M.V.; Vidruk-Nehemya, R.; Herskowitz, M. CO_2 hydrogenation to higher hydrocarbons on K/Fe–Al–O spinel catalysts promoted with Si, Ti, Zr, Hf, Mn and Ce. *Catal. Sci. Technol.* **2017**, *7*, 4048–4063. [CrossRef]
116. Poh, C.K.; Ong, S.W.D.; Du, Y.H.; Kamata, H.; Choong, K.S.C.; Chang, J.; Izumi, Y.; Nariai, K.; Mizukami, N.; Chen, L.W.; et al. Direct methanation with supported MoS_2 nano-flakes: Relationship between structure and activity. *Catal. Today* **2020**, *342*, 21–31. [CrossRef]
117. Qin, S.; Li, J.; Long, J.; Yang, X.; Miao, P. Promotion Effect of Cerium on Mo/Al_2O_3 Catalyst for Methanation. *Appl. Catal. A Gen.* **2020**, *598*, 117559. [CrossRef]
118. Meng, D.J.; Wang, B.W.; Liu, Z.; Wang, W.H.; Li, Z.H.; Ma, X.B. Effects of CeO_2 preparation methods on the catalytic performance of MoO_3/CeO_2 toward sulfur-resistant methanation. *J. Energy Chem.* **2017**, *26*, 368–372. [CrossRef]
119. Wang, B.W.; Yao, Y.Q.; Liu, S.H.; Hu, Z.Y.; Li, Z.H.; Ma, X.B. Effects of of MoO_3 loading and calcination temperature on the catalytic performance of MoO_3/CeO_2 toward sulfur-resistant methanation. *Fuel Process. Technol.* **2015**, *138*, 263–270. [CrossRef]
120. Zhao, J.; Yin, Z.; Wang, B.; Li, Z.; Xu, Y.; Ma, X. Phytic acid-derived fabrication of ultra-small MoP nanoparticles for efficient CO methanation: Effects of P/Mo ratios. *J. Energy Chem.* **2020**, *47*, 248–255. [CrossRef]
121. Varga, G.; Szenti, I.; Kiss, J.; Baan, K.; Halasi, G.; Ovari, L.; Szamosvolgyi, A.; Mucsi, R.; Dodony, E.; Fogarassy, Z.; et al. Decisive role of Cu/Co interfaces in copper cobaltite derivatives for high performance CO_2 methanation catalyst. *J. CO2 Util.* **2023**, *75*, 102582. [CrossRef]
122. Xu, X.L.; Liu, L.; Tong, Y.Y.; Fang, X.Z.; Xu, J.W.; Jiang, D.E.; Wang, X. Facile Cr^{3+}-Doping Strategy Dramatically Promoting Ru/CeO_2 for Low-Temperature CO_2 Methanation: Unraveling the Roles of Surface Oxygen Vacancies and Hydroxyl Groups. *ACS Catal.* **2021**, *11*, 5762–5775. [CrossRef]
123. Panagiotopoulou, P. Methanation of CO_2 over alkali-promoted Ru/TiO_2 catalysts: II. Effect of alkali additives on the reaction pathway. *Appl. Catal. B Environ.* **2018**, *236*, 162–170. [CrossRef]
124. Quindimil, A.; Bacariza, M.C.; González-Marcos, J.A.; Henriques, C.; González-Velasco, J.R. Enhancing the CO_2 methanation activity of γ-Al_2O_3 supported mono- and bi-metallic catalysts prepared by glycerol assisted impregnation. *Appl. Catal. B Environ.* **2021**, *296*, 120322. [CrossRef]
125. Yan, X.L.; Sun, W.; Fan, L.M.; Duchesne, P.N.; Wang, W.; Kubel, C.; Wang, D.; Kumar, S.G.H.; Li, Y.F.; Tavasoli, A.; et al. Nickel@Siloxene catalytic nanosheets for high-performance CO_2 methanation. *Nat. Commun.* **2019**, *10*, 2608. [CrossRef]
126. Pan, Q.S.; Peng, J.X.; Wang, S.; Wang, S.D. In situ FTIR spectroscopic study of the CO_2 methanation mechanism on Ni/$Ce_{0.5}Zr_{0.5}O_2$. *Catal. Sci. Technol.* **2014**, *4*, 502–509. [CrossRef]
127. Xu, X.L.; Tong, Y.Y.; Huang, J.; Zhu, J.; Fang, X.Z.; Xu, J.W.; Wang, X. Insights into CO_2 methanation mechanism on cubic ZrO_2 supported Ni catalyst via a combination of experiments and DFT calculations. *Fuel* **2021**, *283*, 118867. [CrossRef]
128. Miao, B.; Ma, S.S.K.; Wang, X.; Su, H.B.; Chan, S.H. Catalysis mechanisms of CO_2 and CO methanation. *Catal. Sci. Technol.* **2016**, *6*, 4048–4058. [CrossRef]
129. Baraj, E.; Vagaský, S.; Hlinčik, T.; Ciahotný, K.; Tekáč, V. Reaction mechanisms of carbon dioxide methanation. *Chem. Pap.* **2016**, *70*, 395–403. [CrossRef]
130. Su, H.Y.; Yu, C.; Liu, J.X.; Zhao, Y.; Ma, X.; Luo, J.; Sun, C.; Li, W.X.; Sun, K. CO activation and methanation mechanism on hexagonal close-packed Co catalysts: Effect of functionals, carbon deposition and surface structure. *Catal. Sci. Technol.* **2020**, *10*, 3387–3398. [CrossRef]
131. Zhang, J.; Yang, Y.; Liu, J.; Xiong, B. Mechanistic understanding of CO_2 hydrogenation to methane over Ni/CeO_2 catalyst. *Appl. Surf. Sci.* **2021**, *558*, 149866. [CrossRef]
132. Cerdá-Moreno, C.; Chica, A.; Keller, S.; Rautenberg, C.; Bentrup, U. Ni-sepiolite and Ni-todorokite as efficient CO_2 methanation catalysts: Mechanistic insight by operando DRIFTS. *Appl. Catal. B Environ.* **2020**, *264*, 118546. [CrossRef]
133. Westermann, A.; Azambre, B.; Bacariza, M.C.; Graça, I.; Ribeiro, M.F.; Lopes, J.M.; Henriques, C. Insight into CO_2 methanation mechanism over NiUSY zeolites: An operando IR study. *Appl. Catal. B Environ.* **2015**, *174*, 120–125. [CrossRef]
134. Peebles, D.E.; Goodman, D.W.; White, J.M. Methanation of Carbon-dioxide in Ni(100) and the Effects of Surface Modifiers. *J. Phys. Chem.* **1983**, *87*, 4378–4387. [CrossRef]

135. Jacquemin, M.; Beuls, A.; Ruiz, P. Catalytic production of methane from CO_2 and H_2 at low temperature Insight on the reaction mechanism. *Catal. Today* **2010**, *157*, 462–466. [CrossRef]
136. Artz, J.; Muller, T.E.; Thenert, K.; Kleinekorte, J.; Meys, R.; Sternberg, A.; Bardow, A.; Leitner, W. Sustainable Conversion of Carbon Dioxide: An Integrated Review of Catalysis and Life Cycle Assessment. *Chem. Rev.* **2018**, *118*, 434–504. [CrossRef]
137. Hasan, M.; Asakoshi, T.; Muroyama, H.; Matsui, T.; Eguchi, K. CO_2 methanation mechanism over Ni/Y_2O_3: An in situ diffuse reflectance infrared Fourier transform spectroscopic study. *Phys. Chem. Chem. Phys.* **2021**, *23*, 5551–5558. [CrossRef]
138. Wang, F.; He, S.; Chen, H.; Wang, B.; Zheng, L.R.; Wei, M.; Evans, D.G.; Duan, X. Active Site Dependent Reaction Mechanism over Ru/CeO_2 Catalyst toward CO_2 Methanation. *J. Am. Chem. Soc.* **2016**, *138*, 6298–6305. [CrossRef]
139. Schild, C.; Wokaun, A.; Koeppel, R.A.; Baiker, A. CO_2 Hydrogenation over nickel zirconia catalysts from amorphous precursors—On the mechanism of methane formation. *J. Phys. Chem.* **1991**, *95*, 6341–6346. [CrossRef]

Disclaimer/Publisher's Note: The statements, opinions and data contained in all publications are solely those of the individual author(s) and contributor(s) and not of MDPI and/or the editor(s). MDPI and/or the editor(s) disclaim responsibility for any injury to people or property resulting from any ideas, methods, instructions or products referred to in the content.